

# Polarity Reversals from Paleomagnetic Observations and Numerical Dynamo Simulations

Hagay Amit · Roman Leonhardt · Johannes Wicht

Received: 6 April 2010 / Accepted: 31 August 2010 / Published online: 20 October 2010  
© Springer Science+Business Media B.V. 2010

**Abstract** Recent advances in the study of geomagnetic field reversals are reviewed. These include studies of the transitional field during the last geomagnetic reversal and the last geomagnetic excursion based on paleomagnetic observations, and analysis of reversals in self-consistent 3D numerical dynamo simulations. Field models inferred from observations estimate reversal duration in the range of 1–10 kyr (depending on site location). The transitional fields during both the Matuyama/Brunhes reversal and the Laschamp excursion are characterized by low-latitude reversed flux formation and subsequent poleward migration. During both events the dipole as well as the non-dipole field energies decrease. However, while the non-dipole energy dominates the dipole energy for a period of 2 kyr in the reversal, the non-dipole energy merely exceeds the dipole energy for a very brief period during the excursion. Numerical dynamo simulations show that stronger convection, slower rotation, and lower electrical conductivity provide more favorable conditions for reversals. A non-dimensional number that depends on the typical length scale of the flow and represents the relative importance of inertial effects, termed the local Rossby number, seems to determine whether a dynamo will reverse or not. Stable polarity periods in numerical dynamos may last about 1 Myr, whereas reversals may last about 10 kyr. Numerical dynamo reversals often involve prolonged dipole collapse followed by shorter directional instability of the dipole axis, with advective processes governing the field variation. Magnetic upwellings from the equatorial inner-core boundary that produce reversed flux patches at low-latitudes of the core-mantle boundary could be significant in triggering reversals. Inferences from the observational and modeling sides are compared. We summarize with an outlook on some open questions and future prospects.

---

H. Amit (✉)

Laboratoire de Planétologie et de Géodynamique, UMR 6112, Nantes Atlantiques Universités, CNRS, Université de Nantes, 2 rue de la Houssinière, 44000 Nantes, France  
e-mail: [Hagay.Amit@univ-nantes.fr](mailto:Hagay.Amit@univ-nantes.fr)

R. Leonhardt

Central Institute for Meteorology and Geodynamics (ZAMG), Hohe Warte 38, 1190 Vienna, Austria

J. Wicht

Max-Planck-Institut für Sonnensystemforschung, 37191 Katlenburg-Lindau, Germany

**Keywords** Geomagnetic field · Paleomagnetic reconstruction · Geodynamo · Reversal · Excursion · Magnetic dipole · Virtual geomagnetic pole

## 1 Introduction

The geomagnetic field is generated by rapidly rotating convective flows of an electrically-conductive fluid in Earth's outer core in a process known as the geodynamo. Paleomagnetic observations indicate that the field has reversed its polarity hundreds of times in Earth's history. Reversals are rare events in the sense that their duration is much shorter than the length of the stable polarity chrons separating them. Reversals are also very irregular. Their frequency varies significantly, including very long periods of stable polarity. Excursions are another type of event that is characterized by largely anomalous and even inverse local magnetic field directions but fails to establish a lasting polarity change. It is not clear whether reversals and excursions are end members of the secular variation (SV) spectrum, or separate events (Merrill et al. 1998).

Since the pioneering work of Glatzmaier and Roberts (1995b), several studies of numerical dynamo simulations have reported magnetic reversals with some Earth-like features. Despite these increasing efforts, many aspects of the reversal process are still not well-understood. Understanding the nature of geomagnetic field reversals and excursions is important for several reasons:

- Understanding the fundamental mechanisms of the geodynamo—What triggers a reversal and what dynamics and kinematics take place during reversals? Are excursions different from reversals, and if they are, what are the differences?
- Chronology—Substantial peaks in cosmogenic  $^{10}\text{Be}$  and  $^{36}\text{Cl}$  in ice cores from Antarctica and Greenland are attributed to lows in geomagnetic field intensity (Mazaud et al. 1994; Baumgartner et al. 1998) during excursions. The geomagnetic field modulates cosmogenic isotope production in the atmosphere ( $^{14}\text{C}$ ,  $\delta^{18}\text{O}$ ) and thus its most drastic variations, reversals and excursions, have important implications for dating.
- Paleomagnetic data provide the longest un-interrupted time sequence describing the geodynamo.
- Climate variations—Decreases of the geomagnetic field intensity as observed during reversals and excursions might lead to a significant modulation of the magnetosphere and its shielding mechanism (Vogt et al. 2007). A causal relationship between geomagnetic events and climate variation is controversial (Worm 1997; Langereis 1999; Guyodo and Valet 1999).
- Understanding current secular variation—The mechanisms responsible for the present dipole moment rapid decrease, the role of the weak field in the South Atlantic with implications to safety in spaceships and satellite maintenance, and the possibility of a beginning of a new reversal, are still a matter of debate.

Reversals may be investigated using various tools, including numerical models, observations, laboratory magnetohydrodynamics experiments (Berhanu et al. 2007), and theory (Moffatt 1978). In this review we focus on the first two: Numerical modeling of the geodynamo and paleomagnetic observations. Numerical dynamo models have attempted to recover paleomagnetic observations such as chrons and reversals durations, reversal frequency and latitudinal dependence. Only recently paleomagnetic observations reached sufficient quality to enable interpretation in terms of a global field evolution. On the other hand, advances in numerical dynamo modeling provide improved possibilities to investigate

the reversal process. It is now possible to directly compare these two approaches in order to enhance our basic knowledge of these most dramatic variations of the Earth's magnetic field.

Both approaches have their own shortcomings. Paleomagnetic observations suffer from low and inhomogeneous data coverage and uncertain timing, limiting their resolution and reliability. Numerical dynamo models operate in a parameter regime far from what would be appropriate for modeling Earth's core, so their application to the geodynamo is questionable. Therefore the interpretation of paleomagnetic observations and numerical dynamo models and the comparison between the two approaches requires some caution.

In this paper we review recent advances in the study of reversals from two directions. From the observational side, we describe in Sect. 2 recent models of the field during the last geomagnetic reversal and the last geomagnetic excursion. From the modeling side, we highlight in Sect. 3 recent progress in the analysis of reversals in numerical dynamos. Section 4 compares the findings from observations and numerical simulations, and Sect. 5 concludes the paper with a future outlook.

## 2 Observations in Paleomagnetic Data

### 2.1 Paleomagnetic Data and Its Interpretation

More than 100 years ago, volcanic rocks magnetized opposite to the present day field direction were discovered (Brunhes 1906). In the following decades an intriguing discussion about the origin of such inverse direction took place (Smith 1971; Heller 1980). It has been shown that the inverse magnetization of most young volcanic rocks is indeed of geomagnetic origin, although in some rocks partial and full self reversal mechanisms could be found (Schult 1968). The occurrence of such inverse directions in past geological records requires that the Earth's magnetic field reversed its polarity. Today it is well known that such geomagnetic field reversals occurred throughout the Earth's history from Archaean (>3.2 billion yrs) to Quaternary (~775 kys) times. Especially for the Cenozoic and even most of the Mesozoic, a continuous polarity time scale of the magnetic field has been established from geological archives of past geomagnetic field variations (e.g. Cande and Kent 1995). The reversal rate is not constant but changed considerably with time. The total absence of field reversals for several tens of million years is observed during the Cretaceous and the Permian quiet zones. Rather short intervals lasting only a few thousand years have also been observed during the last inverse period, the Matuyama chron. The last few million years are characterized by frequent reversals, on average about four every million years. About 780 kyr ago, the last geomagnetic field reversal caused a transition between a previously inverse polarity field state, the Matuyama chron, to a normal polarity field configuration (the present day polarity) called the Brunhes chron. This normal geomagnetic field polarity has already lasted three times longer than the average reversal frequency of the last 5 Myrs.

To reconstruct past geomagnetic field variations, paleomagnetists mainly use sedimentary and volcanic rocks which acquired a magnetization during deposition/emplacement and stored this signal throughout the geological history. These archives, usually referred to as paleomagnetic records, enable the local geomagnetic field evolution to be inferred even during polarity reversals and excursions. Such records comprise inclination, declination and sometimes a measure of the field intensity. The absolute intensity, however, can only be recovered from volcanic rocks. Many paleomagnetic studies use the concept of a virtual geomagnetic pole (VGP) to describe the field properties. A VGP is an imaginary geocentric dipole that

would explain the locally observed field direction, i.e. inclination and declination (for a defining equation see e.g. Merrill et al. 1998).

Paleomagnetic data provide valuable information about the underlying geodynamo process. Already the simple fact that the geomagnetic field reverses polarity in irregularly spaced intervals constrains the class of possible geodynamo models. Based on paleomagnetic data interpretation, it has been proposed that the geomagnetic field during reversals is not dipole-dominated (Clement 1991), is significantly asymmetric with respect to the equator (Williams and Fuller 1981), and not dominated by axisymmetric components (Hoffman 1981; Theyer et al. 1985; Clement 1991). Some selected records show that VGP paths (Clement 1991; Laj et al. 1991) and volcanic VGP clusters where the VGP lingers for a relatively long period (Hoffman 1992, 1996; Knudsen et al. 2009) seem to prefer two distinct longitude bands along the Americas and roughly  $180^\circ$  away along Australia and East Asia. These aspects are still strongly debated and subject to ongoing research (Valet et al. 1992; Prévot and Camps 1993; Love 1998, 2000; Valet and Herrero-Bervera 2003; Leonhardt and Fabian 2007).

When looking closer into the last normal epoch of the magnetic field since the last field reversal, paleomagnetic records from sediments and volcanic rocks show about a dozen relatively rapid variations in the field directions with VGP tilts exceeding  $45^\circ$  (Lund et al. 2005; Laj and Channell 2007). At least seven of these fast variations, referred to as geomagnetic excursions, are thought to occur globally (Laj and Channell 2007). These excursions do not last longer than a few thousand years and are typically correlated with pronounced lows in paleointensity (Lund et al. 2005; Laj and Channell 2007; Roberts 2008). The origin and nature of geomagnetic excursions have been debated since their discovery, and interpretations range from aborted reversals (Cox et al. 1975; Hoffman 1981; Valet et al. 2008) to anomalous or enhanced paleosecular variation (PSV). Interpretations of the excursions range from rather simple, dipole-dominated structures (e.g. Laj and Channell 2007) to more complex, non-dipole dominated configurations (e.g. Cassata et al. 2008). Because of their very short duration, geomagnetic excursions can be found only in a few paleomagnetic records of adequate temporal resolution (Roberts and Winklhofer 2004).

Low data quality due to questionable remanence recording mechanisms of the rock or insufficient laboratory procedures, uneven global coverage of records, and difficulties in age determination are the limiting factors for the interpretation of paleomagnetic records. Sedimentary records provide a continuous sequence of geomagnetic reversals. Their resolution depends on sedimentation rate and sampling density. The remanence acquisition process in sediments, however, is only partly known. Gradual lock-in over a long time period can lead to smoothing of the geomagnetic field record (Hyodo 1984; Langereis et al. 1992; Bleil and Dobeneck 1999) and to a biased paleointensity distribution (Mazaud 1996). Therefore, sedimentary records are generally considered to be less reliable than volcanic records. The latter, however, often provides only a sequence of discrete data points in time separated by intervals with uncertain duration, because the extrusion rate in the interval between successive lava flows cannot be precisely determined. Thus, a careful investigation of the recording process, the signal stability, deposition conditions and age constraints is necessary to obtain reliable paleomagnetic field records. During the past decades, an increasing amount of high quality paleomagnetic data from spatially distributed sites has become available. Recent advances in paleomagnetic and rock magnetic determination techniques allow the identification of possible sources of errors and provide meaningful quality assessment measures. Radiometric dating techniques for volcanic rocks have improved (Singer et al. 2005) and the dating of sediments is also becoming increasingly more accurate (Langereis et al. 1997;

Laj and Channell 2007). These recent advances in data treatment, spatial coverage and quality, have led to the first global geomagnetic field models during a reversal or an excursion. We review these models in the following sections.

## 2.2 Deriving Global Geomagnetic Field Evolution Models

Principally, one can distinguish between two different types of global field interpretations from paleomagnetic data. The first group primarily extracts dipolar field information from paleomagnetic data, usually in terms of VGPs and/or virtual dipole moments (VDMs). The non-dipolar field components are then either estimated based on the residual field information from the different sites, or simply assumed to resemble the archaeomagnetic field. The latter assumption was used by Brown et al. (2007) and Valet et al. (2008) for analyzing geomagnetic reversal and excursion features. They used the non-dipolar energy variation obtained for the Holocene magnetic field (CALS7k, Korte and Constable 2005) and varied the axial dipolar field to simulate field transitions. Local field variations obtained using this procedure seem qualitatively similar to paleomagnetic records. However, this approach is hampered by the relatively short period covered by the CALS7k model which embraces only a small part of the very rich geomagnetic SV spectrum. Nevertheless, these models demonstrate that many transitional field features that were previously attributed to some specific physical processes in Earth's core can actually be explained by the simple geometric effect of upward continuation of the geomagnetic field (Brown et al. 2007).

The second group of models attempts to reconstruct global magnetic field from paleomagnetic data in terms of spherical harmonics. The spatial complexity of the model, expressed by the maximum degree of the spherical harmonic expansion, is limited by the number of available data points for a given epoch and their global distribution. Obtaining a model up to a certain degree  $\ell$  requires at least  $\ell(\ell - 1)$  evenly distributed data points. Even for low harmonic degrees, such paleomagnetic data spatial coverage and accuracy in time is not available for any reversal or excursion. Therefore, regularization procedures and additional assumptions about the reversal process are needed. Mazaud (1995) and Shao et al. (1999) were the first to present reconstructions of transitional fields which are predominantly based on paleomagnetic data and less on assumptions about the reversal process itself. Both studies are based solely on paleomagnetic directional data from geomagnetic field reversals, namely the Olduvai/Matuyama and the last geomagnetic reversal, the Matuyama/Brunhes. They do not use paleointensity estimates. A common relative age model for the different sites is established by correlating similar features from spatially separate records. To invert for the Gauss coefficients of the spherical harmonics model, additional constraints are then used. For example, Mazaud (1995) require constant energy at the core-mantle boundary (CMB) (for a brief overview on global field reconstructions see Leonhardt and Fabian 2007).

Pre-inversion time correlation of paleomagnetic features, using either relative paleointensity estimates or directional variations in terms of VGP latitude, have also been used in recent models of the Iceland basin excursion (Lanci et al. 2008) and the Matuyama/Brunhes reversal (Ingham and Turner 2008). A different approach, without any a priori constraints on synchronous paleomagnetic features was postulated by Leonhardt and Fabian (2007). Their iterative Bayesian inversion technique has been applied to models of the Matuyama/Brunhes reversal (IMMAB4, Leonhardt and Fabian 2007) and the Laschamp excursion (IMOLEe, Leonhardt et al. 2009). In this approach, an initial paleomagnetic data set is inverted under the constraint that the power in the magnetic energy SV spectrum is minimized. A Bayesian

inversion corresponds to minimizing the quantity

$$\frac{1}{2} \sum_i \left( \frac{\mathbf{B}_i + \nabla \Phi(\mathbf{G}_\Gamma(t_i), \theta_i, \phi_i)}{\Delta \mathbf{B}_i} \right)^2 + \frac{1}{\Delta \mathfrak{P}_0} \int_0^1 \sum_{\ell=1}^L R_\ell(\partial_t \mathbf{G}_\Gamma(t)) dt = \min. \tag{1}$$

The first term in (1) is related to the difference between observed paleomagnetic data and the modeled spherical harmonic expansion  $\Phi(\mathbf{G}_\Gamma(t_i), \theta_i, \phi_i)$ , where  $\mathbf{G}_\Gamma(t_i)$  are the Gauss coefficients,  $t_i$  time and  $(\theta_i, \phi_i)$  the location. The evolution matrix  $\Gamma$  contains the information describing the field change from its initial to final state before and after the reversal (see Leonhardt and Fabian 2007).  $\mathbf{B}_i = \mathbf{B}(t_i, \theta_i, \phi_i)$  denotes full vector paleomagnetic data with related Gaussian error  $\Delta \mathbf{B}_i = \Delta \mathbf{B}(t_i, \theta_i, \phi_i)$ . The Gaussian error should be obtained by uncertainty analysis of individual paleomagnetic sites. Although such uncertainties are not yet available, tests using different uncertainties for each record show that the Gaussian error is not crucial in determining the model complexity.

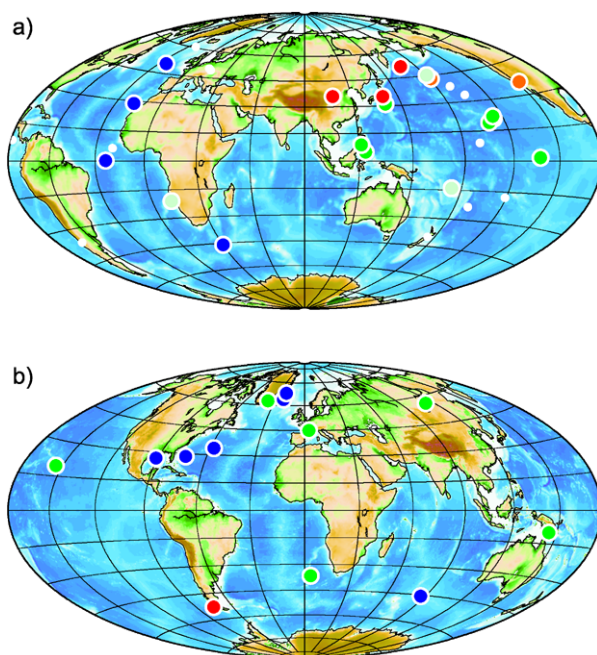
The second term describes the regularization function using the regularization parameter  $\Delta \mathfrak{P}_0$  which controls the trade-off between energy fluctuation minimization and data fitting. The product of the Mauersberger-Lowes magnetic SV spectrum (Allredge 1984) and the time increment  $dt$ , termed here the variational power, is

$$R_\ell(\partial_t \mathbf{G}(t)) dt = (\ell + 1) \sum_{m=0}^{\ell} [\partial_t g_\ell^m(t)^2 + \partial_t h_\ell^m(t)^2] dt. \tag{2}$$

After inverting an initial record, iteratively additional records are included by correlating full vector field variations from model predictions and the newly added paleomagnetic data. This technique requires at least one absolute paleointensity record to calibrate relative intensity measures from sedimentary records. The obtained models are based on a sub-collection of the available paleomagnetic records for a specific polarity transition and are then tested against the remaining independent data sets.

An important remaining question is, whether the information contained in the paleomagnetic data suffices to resolve the transitional field reliably. This question involves several aspects. First, the spatial and temporal distribution of paleomagnetic records is poor for most reversals and excursions. As can be seen in Fig. 1, even for the best resolved reversal (Matuyama/Brunhes) and excursion (Laschamp), large regions are without any record and data from the southern hemisphere are very rare. In particular, full vector records providing absolute paleointensity estimates are missing for most reversals and excursions. For the Bayesian approach such records are essential since all relative intensity measurements are calibrated against an absolute intensity record. Second, any reconstruction method is affected by uncertainties in the paleomagnetic data. This primarily concerns relative and absolute intensity values which can be significantly biased by a number of different factors. Any reconstruction should thus rely only on records where tests have shown minimal bias. Finally, dating and chronology are problematic. Sedimentary data sets are often dated by oxygen chronology or tuned based on Milankovic cycles. Volcanic records are dated by radiometric methods providing age estimates for individual lavas. Combining different records by either correlating features in the record or using an iterative approach also combines different age models. Usually, only one age model of a single data set is then chosen to represent the ages in the final model. Thus the models' chronology depends on the accuracy of this age determination of the paleomagnetic data sets. As shown below, different modeling approaches (Shao et al. 1999; Leonhardt and Fabian 2007;

**Fig. 1** Sampling locations of paleomagnetic data from the Matuyama/Brunhes reversal (a) and the Laschamp excursion (b). Brown colors indicate volcanic records. Sedimentary data is distinguished into sea sediments (yellow), lake sediments (light yellow) and löss (turquoise). Only colored locations were used by Leonhardt and Fabian (2007)



Ingham and Turner 2008) using different data collections, record alignments and regularization functions exhibit many common features in the final reversal model. All these approaches accounted for the above problems to some extent. Nevertheless, the availability of high quality paleomagnetic records is very limited. In order to better spatially constrain global paleomagnetic field reconstructions and to verify some modeling assumptions (e.g. intensity calibration), additional records are indispensable.

### 2.3 Characteristics of Geomagnetic Field Reversals

The last reversal, the Matuyama/Brunhes which occurred about 780 kyr ago, is by far the best documented polarity transition in terms of amount, spatial coverage and quality of available paleomagnetic records (Fig. 1a). More than 50 records are currently available, of which several more reliable sub-collections were established (Love and Mazaud 1997; Clement 2004). Figure 1a shows the records used for constructing the IMMAB4 model of Leonhardt and Fabian (2007) and the sites used for testing the model's prediction, which is essentially the collection of Clement (2004). Due to the relatively large amount of spatially distributed data sets, the Matuyama/Brunhes transition is the best candidate for paleomagnetic reconstruction of global geomagnetic field variations during polarity transitions (Shao et al. 1999; Leonhardt and Fabian 2007; Ingham and Turner 2008). Different reconstruction approaches use different selections of high quality records from the available data sets. Figure 2 shows the site distribution as well as some comparisons of field prediction and paleomagnetic data for the IMMAB4 model.

Using different records from the available data set, Shao et al. (1999) and Ingham and Turner (2008) constructed global time-evolution models up to degree three, whereas IMMAB4 of Leonhardt and Fabian (2007) is expanded up to degree four. Thus a general description of the field variation is obtained which enables analyzing the field morphology

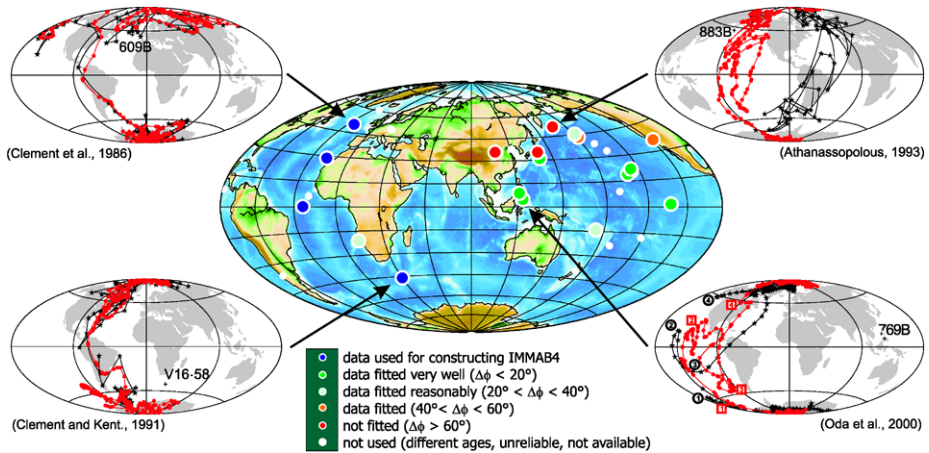


**Fig. 2** Comparison of paleomagnetic data (*black*) and its field prediction by the IMMAB4 model (*red*) for sampling locations of the last geomagnetic reversal. The *color codes* on the *locations map* indicate differences between the predicted and observed average VGP latitude of transitional directions ( $\Delta\phi$ )

during the reversal. IMMAB4 was verified by testing its field prediction on independent paleomagnetic records. Most records from the collection of Clement (2004) are predicted reasonably well in terms of transitional VGP movement, duration and intensity variation (Leonhardt and Fabian 2007).

### 2.3.1 Field Morphology of a Reversal

It is strongly debated and of much physical interest to know how low the dipole decreases and what is the behavior of the non-dipole field during a reversal (see Merrill and McFadden 1999 and references therein). To address this question, the dipole and non-dipole contributions to the magnetic energy at the Earth's surface during the reversal as calculated by the IMMAB4 model are plotted in Fig. 3, accompanied by two snapshots of the radial field component at the CMB. A difference between the proportion of dipole and non-dipole terms of the pre-transitional and the post-transitional fields is clearly visible. Prior to the reversal, at around 785 kyr of the IMMAB4 time scale, the non-dipolar energy is increasing towards the dipolar level. At the CMB, reversed flux patches form at the equator and move poleward. At around 780 kyr, the non-dipolar energy reaches its maximum (MB1, Fig. 3). In the following, dipolar and non-dipolar energies jointly decrease at similar rates towards the dipole minimum. Here, the field within the tangent cylinder (the imaginary cylinder parallel to the rotation axis and tangent to the inner-core boundary, from hereafter TC) of the southern hemisphere reverses, heralding the global field reversal. Within the northern hemisphere TC the field remains in its pre-transitional polarity until  $\sim 3$  kyr after the dipole minimum (MB2, Fig. 3). After this final local polarity change, a gradual increase of the dipole energy towards the pre-transitional value is found. For about 2 kyrs, around 775 kyr, the dipolar energy drops drastically well below the non-dipolar level. While the dipole recovers after this drop, the non-dipole continues to drop. The field evolution before 785 kyr and after 767 kyr is not well resolved by the IMMAB4 model because of poor paleomagnetic data coverage.

Similar features, particularly the formation of low-latitude reversed flux patches prior to the reversal as well as their positions throughout the transition, are obtained by Shao et al. (1999) and Ingham and Turner (2008). In particular, patches of outward directed field near

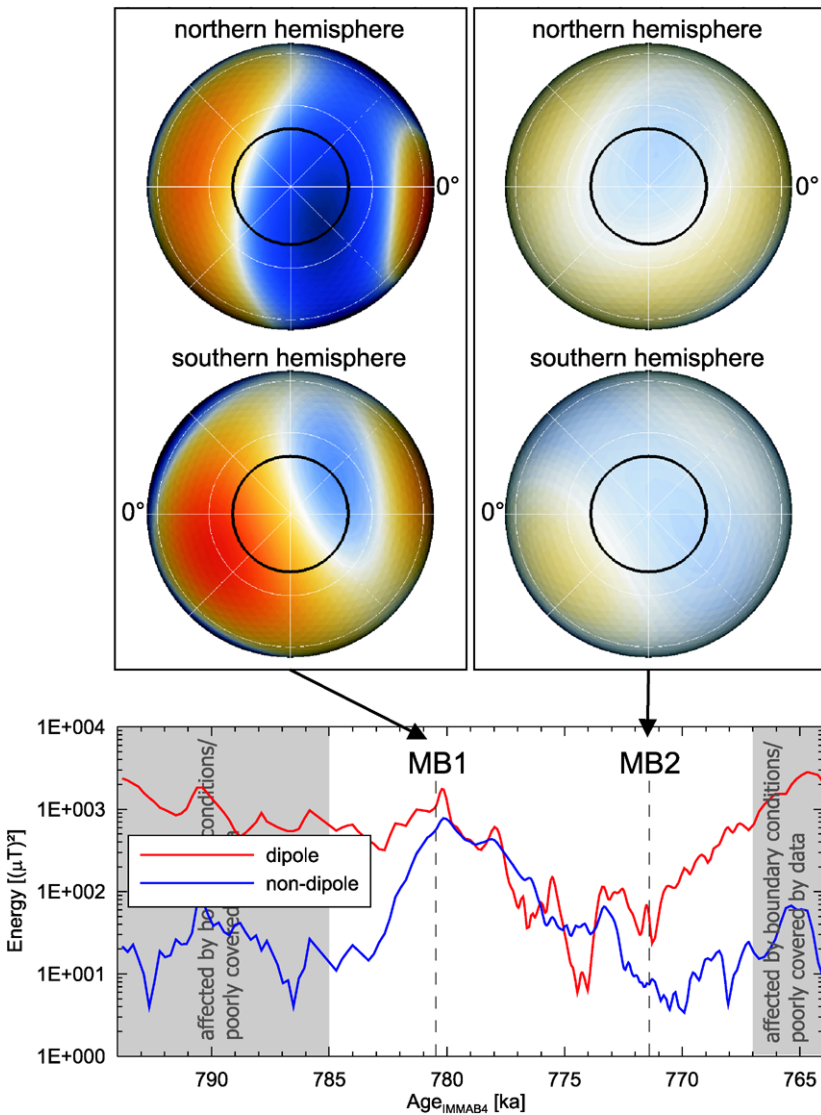


**Fig. 3** The field evolution during the last reversal according to Leonhardt and Fabian (2007). Dipolar and non-dipolar energies are shown for the Earth’s surface. Two snapshots show the field configuration at the CMB. Here, red shades indicate inward, blue shades outward-directed radial field. The IMMAB4 timescale is based on the 664D sedimentary core (Valet et al. 1989; Lisiecki and Raymo 2005) and average Ar/Ar age of the Haleakala sequence (Singer et al. 2005). In the northern/southern hemispheres, 90°E is at the top/bottom respectively. The black circles mark the tangent cylinder

South America and in the Indian Ocean as well as inward flux at the Greenwich meridian, are found almost identically in all three reversal models, which are based on different data collections and different modeling methods. In addition to the independent verification test, this agreement demonstrates that the field models extracted by the inversion of the paleomagnetic data are relatively independent of the data selection, and thus strength-

ens the confidence in these models. The model of Ingham and Turner (2008) includes a pre-transitional field excursion approximately 20 kyr prior to the Matuyama/Brunhes transition. Like the subsequent reversal, this excursion appears to start similarly by formation of low-latitude reversed flux patches. During the IMMAB4 reversal, the most significant non-dipolar contribution comes from the  $\ell = m = 2$  field components.

### 2.3.2 Implications of Paleomagnetic Observations of Reversals

Several inferences on the transitional geomagnetic field behavior, usually drawn from selected paleomagnetic records, are strongly debated. Among these open questions is the existence of meta-stable transitional field states (Hoffman 1992). Transitional clusters of VGPs, suggesting such a meta-stable state, are often observed in volcanic records but not in sediments. These clusters, however, could also be related to intense volcanic activity producing numerous lava flows in a relatively short time interval (Prévot and Camps 1993). On the other hand, the continuous VGP paths observed in sedimentary records can be related to delayed remanence acquisition, which removed the clustering signal. The global field models of Leonhardt and Fabian (2007) and Ingham and Turner (2008) suggest that both types, VGP clusters and continuous paths, have occurred during the last reversal, and that the type of observation depends on the site location relative to emerging prominent geomagnetic flux patches during the reversal. Furthermore, a preference for two longitudinal bands as observed in selected sedimentary records and some volcanic records (e.g. Laj et al. 1991; Hoffman 1992) is not supported by IMMAB4. Here, transitional VGPs of equally distributed sites show a preference for only a single longitude band in the Pacific.

From a paleomagnetic perspective, the duration of a reversal is estimated based on directional data alone, for example the time it takes for the VGP to move between latitudes  $45^\circ$  north and  $45^\circ$  south. Since non-dipolar contributions seem to be significant during the reversal, reversal duration estimate strongly depends on site location (Clement 2004). The IMMAB4 model suggests large duration differences ranging from  $\sim 1$  kyr up to more than  $\sim 10$  kyrs (Leonhardt and Fabian 2007). Apart from variations in duration, the paleomagnetic age of the last reversal, defined by the equatorial crossing of the VGP, also varies with site location (Leonhardt and Fabian 2007; Ingham and Turner 2008). Finally, while the local field intensity can drop below 10% of the pre-transitional values at some locations and times, it can also remain fairly strong at a few locations for some period during the transition. Such range is found in many detailed paleomagnetic observations (e.g. Prévot et al. 1985; Leonhardt and Soffel 2002).

## 2.4 Characteristics of Geomagnetic Field Excursions

The Laschamp excursion, originally discovered in 1967 (Bonhommet and Babkine 1967) in lava flows from the Chaîne des Puys in France, is the best examined geomagnetic excursion (Fig. 1b). It has been confirmed as a global excursion that occurred approximately 41 kyr ago and has been found in several sedimentary and volcanic sequences (Levi et al. 1990; Kissel et al. 1999; Laj et al. 2000; Guillou et al. 2004; Krása et al. 2005; Lund et al. 2005; Channell 2006; Laj et al. 2006; Cassata et al. 2008).

Using a similar approach as for the last geomagnetic reversal, the iterative Bayesian inversion was applied to six paleomagnetic records to model the Laschamp excursion (IMOLEe, Leonhardt et al. 2009). Hereby, a spherical harmonic model up to degree five was derived for the temporal geomagnetic field variation between 43.5 kyr and 36.5 kyr before present. The distribution of available records and a comparison of paleomagnetic data

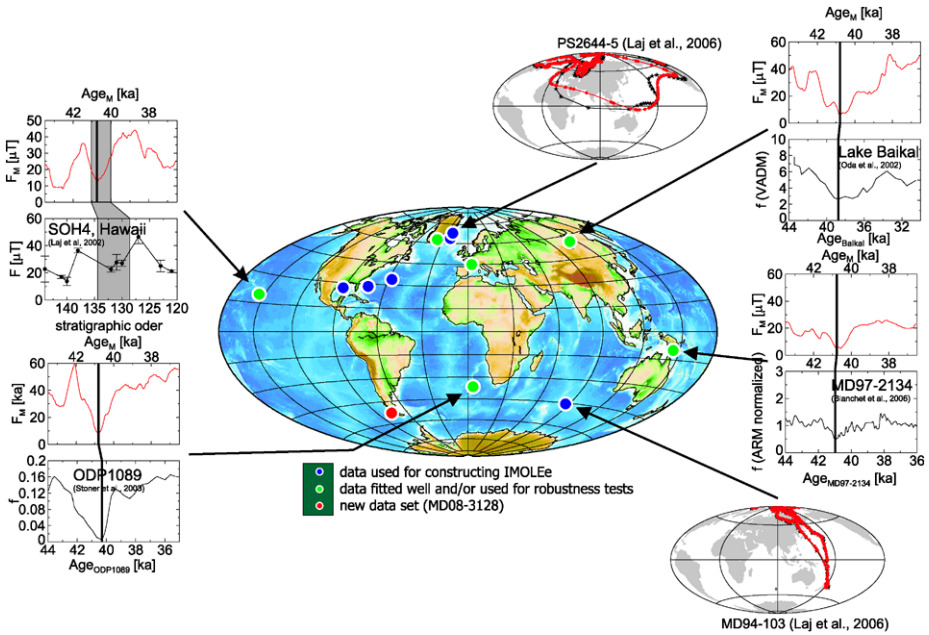


**Fig. 4** Comparison of paleomagnetic data (black) and its field prediction by the IMOLEE model (red) for sampling locations of the Laschamp excursion. The color codes in the location maps qualitatively indicate how well the data is fitted by IMOLEE

with model predictions is shown in Fig. 4. The model predicts very well independent paleomagnetic records that were not used for the inversion and is fairly insensitive to modeling parameters and data selection (see Fig. 4 and Leonhardt et al. 2009). The current data collection, however, is dominated by records from the northern hemisphere, particularly from the North Atlantic. A better spatial coverage with additional constrain records from the southern hemisphere and the Pacific region is necessary to better constrain the model.

2.4.1 Field Morphology of an Excursion

Figure 5 shows dipolar and non-dipolar field temporal evolutions at the Earth’s surface and the field morphology for the Laschamp excursion (for comparison with the reversal, see the corresponding Fig. 3). The IMOLEE time scale, indicated by a subscripted  $M$ , is based on the piston core PS2644-5 taken on a Polarstern cruise (Laj et al. 2006). Approximately 2 kyr before the dipole minimum, which may be defined as roughly the center of the excursion, dipolar and non-dipolar energies start to decrease simultaneously. Already at the beginning of the decrease (LE1, LE2), large-scale reversed flux patches are present close to the equator. In the Eastern Pacific, inward directed flux forms south of the equator and an outward-directed patch is found in the northern hemisphere below North America. This pair of reversed flux patches gradually moves poleward prior to the excursion (LE2, LE3). Both patches stop at the TC. Another pair of reversed patches is seen below Russia and Indonesia, roughly 180° away from the eastern Pacific pair, but the latter is somewhat less prominent. The dipolar energy reaches its minimum at 40.8 kyr, shortly after the non-dipolar energy. For a brief interval of less than 200 years $_M$ , the non-dipolar energy prevails, mainly

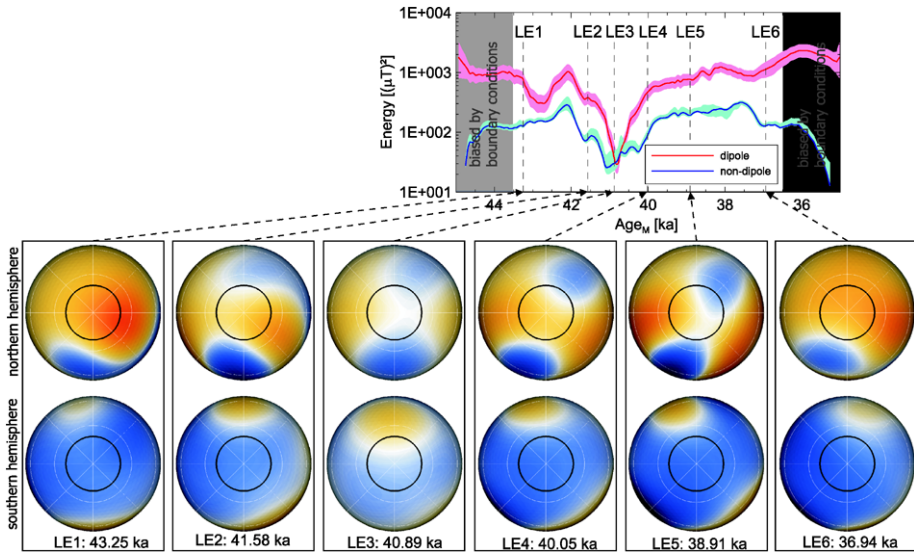


**Fig. 5** A series of snapshots depicting the field evolution at the CMB during the Laschamp excursion (Leonhardt et al. 2009). Red shades indicate inward, blue shades outward-directed radial field. The IMOLEe time scale, indicated by a subscripted  $M$ , is based on PS2644-5 (Laj et al. 2006). In the northern/southern hemispheres,  $90^\circ E$  is at the top/bottom respectively. The black circles mark the tangent cylinder

due to strong  $\ell = 3 \ m = 2$  components. Afterwards, both energy contributions gradually increase. Throughout the excursion the field within the TC in both hemispheres is dominated by normal polarity flux.

Similar field morphologies during an excursion are found by other studies. Low-latitude flux patches at the onset of an excursion are observed in the spherical harmonic model of the Matuyama/Brunhes precursor at  $\sim 795$  kyr (Ingham and Turner 2008). Data from the Iceland basin excursion (Lanci et al. 2008) also suggest only a very short period ( $\sim 1$  kyr) of non-dipolar dominance.

#### 2.4.2 Implications of Paleomagnetic Observations of Excursions

As with IMMAB4, IMOLEe demonstrated that the magnetic field records across the Laschamp excursion depend on site location. However, the spatial differences in IMOLEe are much smaller than in IMMAB4 due to the stronger dipole contribution and the shorter interval of non-dipolar dominance. Nevertheless, these local discrepancies are of major interest for paleomagnetism and chronostratigraphy. While at most sites the field intensity drops to about 10–20% of the pre-transitional values close to the dipole minimum, in some regions like the Pacific relatively large intensities are retained. This IMOLEe prediction is consistent with independent paleomagnetic observations in Hawaii (Laj et al. 2002) although the ages for the paleomagnetic data are not well constrained. According to IMOLEe, lowest intensities are observed 2 kyr $_M$  prior to the Laschamp excursion in Hawaii. Temporal deviations of the intensity minimum are also observed for other regions. Such variations could lead to chronostratigraphic errors when intensity minima are used to correlate distant records.

Estimates using the observational range of excursions directions indicate an average Laschamp duration of 1.1 kyrs. In some regions, durations above 2 kyrs and well below 1 kyr

are observed. It has also been noted for sedimentary records that the Laschamp excursion can often be identified in the relative paleointensity signal, even if the directional paleomagnetic field signal shows no anomalous variation, for example the high quality records from the South Atlantic (Stoner et al. 2003) and the equatorial West Pacific (Blanchet et al. 2006). The absence of a directional excursion signature is commonly attributed to smoothing by the sedimentary remanence acquisition process (Roberts and Winklhofer 2004). However, particularly in the West Pacific, IMOLEe predicts that the excursions field directions indeed should not significantly deviate from the normal PSV range. Therefore, the observed absence may be a truly recorded geomagnetic signal.

## 2.5 Comparing Reversal and Excursion from an Observational Perspective

When comparing the model of the Laschamp excursion with that of the Matuyama/Brunhes reversal, several similarities are observed. In both cases the field instability starts when reversed flux patches form in equatorial to mid-latitude regions at the CMB, and then move poleward (Leonhardt and Fabian 2007; Ingham and Turner 2008; Leonhardt et al. 2009). Furthermore, the non-dipole energy exceeds the dipolar energy for a brief time interval in both events, which coincides with the time at which the reversal (i.e. the maximum of the directional excursion) is observed at most locations on Earth. This non-dipolar dominance provokes a site dependence of paleomagnetic observations on the Earth's surface leading to variations in duration and age estimates as well as different variations in direction and intensity.

In contrast, a number of significant differences between a reversal and an excursion are also observed. In the excursion scenario, dipolar and non-dipolar energies decrease simultaneously prior to the excursion. The non-dipolar energy remains well below the dipolar energy. In the reversal model, however, the non-dipolar energy increases prior to the polarity change until it reaches the level of the dipolar energy. From then on, both terms coherently decrease until the field reverses at the dipole minimum. When the non-dipole energy reaches the level of the dipole energy, the field within the TC of the southern hemisphere starts to reverse, the quadrupole increases strongly, and additional equatorial flux patches add further complexity to the non-dipolar field. In the case of the excursion, the field within the TC remains of the same polarity throughout the modeled time period. These observations support theoretical considerations and inferences from dynamo models, which indicate that the inner and outer regions of the TC belong to different hydrodynamic regimes, and that this separation influences the structure of large-scale geomagnetic variations (e.g. Olson et al. 1999). Furthermore, the observed differences suggest that the nature of an upcoming field instability is already expressed in the structure of the field energy prior to the dipole minimum (Leonhardt et al. 2009). Both events are triggered by the formation of low- to mid-latitude reversed flux patches that move poleward. However, if the non-dipole energy remains during most of the event significantly lower than the dipole energy, the field within the TC remains unchanged, the flux patches decay away without any long-lasting polarity transition, and this scenario develops into a geomagnetic excursion. If, however, the non-dipole field increases with respect to the dipole, reversed flux patches appear within the TC (at least in one hemisphere), and this scenario leads to a geomagnetic field reversal. If it is indeed possible to predict whether a dipole collapse event will result in a reversal or an excursion based on the relative dipole to non-dipole energies prior to the dipole minimum, then the idea that excursions are nothing more than aborted reversals is wrong, and in fact the two processes are inherently different in nature.

During the Matuyama/Brunhes field reversal (IMMAB4), the non-dipole terms strongly dominate for a significant time interval of 2 kyrs. The surface geomagnetic field is therefore of high complexity, leading to strongly varying paleomagnetic observations. During the excursion (IMOLEe), the non-dipole dominance is less significant and lasts only 10% of the event’s duration. The paleomagnetic observations are less complex and similar surface observations are to be expected for large regions (Laj et al. 2006).

### 3 Numerical Dynamo Models

#### 3.1 Introduction

Numerical dynamos are 3D self-consistent models that solve the full set of magnetohydrodynamics equations for dynamo action due to an electrically-conducting, convecting fluid in a rotating spherical shell (e.g. Olson et al. 1999). These models are solutions for the disturbance around a well mixed adiabatic background state and typically assume the Boussinesq approximation, in which any density and temperature variations in the background state is ignored. The non-dimensional fundamental equations include the momentum equation

$$E \left( \frac{\partial \vec{u}}{\partial t} + \vec{u} \cdot \nabla \vec{u} - \nabla^2 \vec{u} \right) + 2\hat{z} \times \vec{u} + \nabla P = Ra \frac{\vec{r}}{R} T + \frac{1}{Pm} (\nabla \times \vec{B}) \times \vec{B}, \tag{3}$$

the magnetic induction equation

$$\frac{\partial \vec{B}}{\partial t} = \nabla \times (\vec{u} \times \vec{B}) + \frac{1}{Pm} \nabla^2 \vec{B}, \tag{4}$$

the heat equation

$$\frac{\partial T}{\partial t} + \vec{u} \cdot \nabla T = \frac{1}{Pr} \nabla^2 T, \tag{5}$$

the continuity equation

$$\nabla \cdot \vec{u} = 0, \tag{6}$$

and the no-monopole field equation

$$\nabla \cdot \vec{B} = 0 \tag{7}$$

where  $\vec{u}$  is the velocity,  $\vec{B}$  is the magnetic field,  $T$  is temperature,  $t$  is time,  $\hat{z}$  is a unit vector in the direction of the rotation axis,  $P$  is the modified pressure that also accounts for the centrifugal force,  $\vec{r}$  is the position vector and  $R$  is the shell outer radius. The variable  $T$  can be generalized as buoyancy, so that both thermal and compositional convection can be considered given appropriate boundary conditions.

Four non-dimensional parameters in (3)–(7) control the system. The (modified) Rayleigh number  $Ra$  scales the strength of the buoyancy force driving the convection relative to retarding forces

$$Ra = \frac{\alpha g_0 \Delta T D}{\nu \Omega} \tag{8}$$

where  $\alpha$  is thermal expansivity,  $g_0$  is gravitational acceleration on the outer boundary,  $\Delta T$  is temperature difference between the inner and outer boundaries,  $D$  is shell thickness,  $\nu$

is kinematic viscosity, and  $\Omega$  is rotation rate. The Ekman number  $E$  represents the ratio of viscous and Coriolis forces

$$E = \frac{\nu}{\Omega D^2}, \quad (9)$$

the Prandtl number  $Pr$  is the ratio of kinematic viscosity to thermal diffusivity  $\kappa$

$$Pr = \frac{\nu}{\kappa} \quad (10)$$

and the magnetic Prandtl number  $Pm$  is the ratio of kinematic viscosity to magnetic diffusivity  $\lambda$

$$Pm = \frac{\nu}{\lambda}. \quad (11)$$

Several important output parameters characterize the dynamo models. The magnetic Reynolds number  $Rm$  represents the ratio of magnetic advection to magnetic diffusion in the induction equation (4)

$$Rm = \frac{UD}{\lambda} \quad (12)$$

where  $U$  is a typical velocity magnitude. The Elsasser number  $\Lambda$  is the conventional measure of the ratio of Lorentz to Coriolis forces in the momentum equation (3)

$$\Lambda = \frac{\sigma B^2}{\rho \Omega} \quad (13)$$

where  $\sigma$  is electrical conductivity,  $B$  is a typical magnetic field strength and  $\rho$  is fluid density. We note that the Elsasser number relies on a balance between magnetic advection and diffusion in the induction equation, while in frozen-flux conditions at which magnetic diffusion is negligible (Roberts and Scott 1965) the Lenhart number is more appropriate (Jault 2008). The local Rossby number is

$$Ro_\ell = \frac{\ell_u U}{\pi \Omega D} \quad (14)$$

where the typical spherical harmonic degree of the flow  $\ell_u$  is defined as (Olson and Christensen 2006)

$$\ell_u = \frac{\sum_{\ell=0}^{\ell_{max}} \ell \langle \vec{u}_\ell \cdot \vec{u}_\ell \rangle}{\langle \vec{u} \cdot \vec{u} \rangle} \quad (15)$$

In (15)  $\vec{u}_\ell$  is the spherical harmonic degree  $\ell$  component of the velocity  $\vec{u}$  and  $\langle \rangle$  denotes the rms value in the volume of the spherical shell.

Following Glatzmaier (1984) and Glatzmaier and Roberts (1995a), most numerical dynamos operate with a pseudospectral method in which Chebyshev polynomials are used in the radial direction and spherical harmonics in the horizontal direction. This allows expressing partial derivatives analytically. Non-linear terms and the Coriolis force are solved on numerical grid points and then transferred into respective spectral representations. The magnetic and velocity fields are represented by a toroidal/poloidal decomposition which replaces the three vector components with two potentials and guarantees zero divergence. For more details see Christensen and Wicht (2007).

Due to computational limitations, numerical dynamos operate in a parametric regime very far from Earth-like conditions (e.g. Glatzmaier 2002). Based on molecular (rather than

**Table 1** Setup of three dynamo models frequently discussed in the paper. Case T is from Aubert et al. (2008b), case T4 from Wicht et al. (2009) and Case C from Olson et al. (2009). Thermal/compositional convection types are denoted by ‘temp’/‘chem’ respectively. The control parameters are the Ekman  $E$ , Rayleigh  $Ra$ , magnetic Prandtl  $Pm$  and Prandtl  $Pr$  numbers. Also given some output parameters: The magnetic Reynolds number  $Rm$ , the dipolarity  $d$  and the local Rossby number  $Ro_\ell$ . For Earth’s core: Estimate of  $Rm$  was obtained by assigning typical geomagnetic westward drift for the velocity scale (Blokhin and Jackson 1991), the value of  $d$  was calculated from a modern geomagnetic field model (Stacey 1992), and  $Ro_\ell$  was extrapolated using a scaling law derived from numerical dynamo models (Olson and Christensen 2006)

Case	Conv.	$E$	$Ra$	$Pm$	$Pr$	$Rm$	$d$	$Ro_\ell$
T	temp	$2 \cdot 10^{-2}$	$1.75 \cdot 10^4$	10	1	110	0.35	0.27
T4	temp	$1 \cdot 10^{-3}$	$5 \cdot 10^5$	10	1	435	0.2	0.12
C	chem	$6.5 \cdot 10^{-3}$	$1.9 \cdot 10^4$	20	1	112	0.55	0.04
Core	temp/chem	$10^{-14}$	$10^{24}$	$10^{-6}$	1	500	0.64	0.09

turbulent) diffusivities, the Ekman number in most dynamo models is about 8–10 orders of magnitude larger than in Earth’s core, the magnetic Prandtl number is about 4–6 orders of magnitude too large, and the supercriticality of the Rayleigh number is 2–3 orders of magnitude too small (Christensen and Aubert 2006). Nevertheless, and perhaps surprisingly, numerical dynamo models recover rather well some important spatial and temporal features of the geodynamo. Moreover, the magnetic Reynolds number and the Elsasser number in dynamo models are on the same order of magnitude as in Earth’s core, which can be interpreted as successful measures for the flow and field strengths.

Reversing dynamo models were found at vastly different control parameters and also for different convective driving modes. In Table 1 we list the convection type, control parameters and some output parameters of three reversing models that are lengthily discussed below. Models T (Aubert et al. 2008b) and T4 (Wicht et al. 2009) are driven by fixed buoyancy boundary conditions without any internal heat sources. This can be interpreted as purely thermal driving by the latent heat released from a growing inner core. Model C (Olson et al. 2009) mimics compositional convection by imposing zero buoyancy flux at the outer boundary, fixed buoyancy flux at the inner boundary, and a volumetric sink. This corresponds to light elements released from the growing inner core and mixed into the fluid outer core. All three models use relatively large Ekman numbers, which yields solutions with rather large length scales. This permits long simulation runs which capture the statistically rare reversal events, and also eases the analysis of the models’ output. Given the Ekman number, Rayleigh and magnetic Prandtl numbers are adjusted to yield a reversing dynamo with large enough magnetic Reynolds numbers for obtaining a strongly time-dependent field with chaotic reversals. Note that  $Rm$  is typically on the small side for lower  $E$  models (this could, however, be remedied by further increasing  $Pm$ ). Model T4 is more realistic than the other two in terms of its larger  $Rm$ , but less realistic than the other two in terms of its lower dipolarity value. Compositional driving enables reversing dynamos to reach more dipolar fields during chrons (Kutzner and Christensen 2002; Wicht and Olson 2004; Olson 2007). In addition, the inertial effect is significantly weaker in model C than in models T and T4, with  $Ro_\ell$  for case C being below the transitional value from stable to reversing dynamos (see Table 1). In the next section we describe in greater details how the ability of dynamo models to reverse depends on the control parameters, the type of convection and the form of the applied boundary conditions.

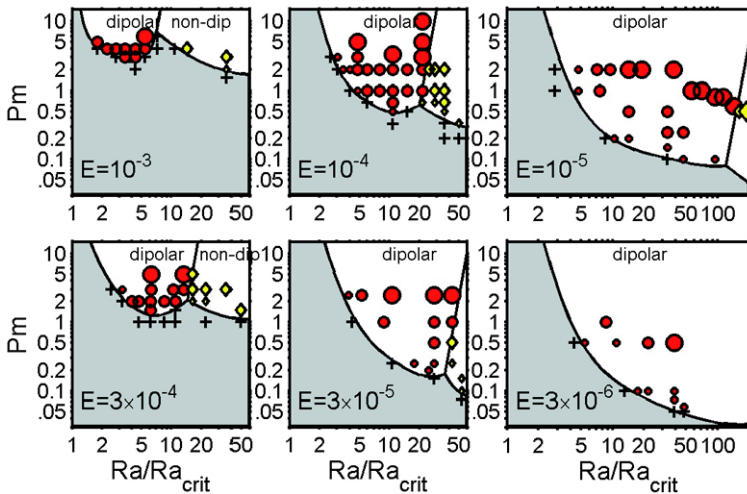


**Fig. 6** Diagram showing regimes of no dynamo (*crosses*), stable dipolar dynamos (*red circles*), and reversing multipolar dynamos (*yellow diamonds*) for various Ekman ( $E$ ) numbers as a function of Rayleigh ( $Ra$ ) and magnetic Prandtl ( $Pm$ ) numbers (U. Christensen, personal communication). The size of the *symbols* represents the relative magnetic field strength

### 3.2 Conditions for Reversing Dynamos

Systematic studies of numerical dynamos provide vital information about the dependence of dynamo properties on the system parameters (Christensen et al. 1999; Kutzner and Christensen 2002; Christensen and Aubert 2006; Takahashi et al. 2008). For our purposes, these studies enable to uncover the favorable conditions for dynamos to reverse in terms of the control parameters. An updated state of the results of the systematic parametric study of Christensen and Aubert (2006) with fixed temperature boundary conditions is shown in Fig. 6 (kindly provided by Uli Christensen). When varying the Rayleigh number ( $Ra$ ) and magnetic Prandtl number ( $Pm$ ) while keeping the Ekman number ( $E$ ) and the Prandtl number ( $Pr$ ) fixed, three different dynamo regimes can be distinguished in Fig. 6: a regime where no dynamo action is maintained (*crosses*), a regime with dipole dominated dynamos (*red circles*), and a regime with multipolar dynamos (*yellow diamonds*). The dipolar dynamos never switch polarity, while the weaker axial dipole contribution in the multipolar cases reverses rather frequently. Dipole dominated dynamos that rarely reverse can in some cases be found at the boundary between both regimes. We come back to discussing these somewhat more Earth-like reversing cases in the next section.

Increasing  $Ra$  and/or  $Pm$  results in the transition from non-magnetic convection to dynamos. Larger  $Ra$  yield more vigorous flows while larger  $Pm$  are synonymous to smaller magnetic diffusivities. An increase in either parameter therefore raises the magnetic Reynolds number ( $Rm$ ) and will ultimately lead to the onset of dynamo action when  $Rm$  exceeds a critical value. The respective trade-off in  $Ra$  and  $Pm$  is apparent in Fig. 6. As convection becomes more vigorous, i.e. larger  $Ra$  values, the magnetic variability increases and eventually a transition from stable dipolar to reversing multipolar dynamos takes place. The dependence of reversibility on  $Pm$  is less trivial. As seen in Fig. 6, the boundary between the dipolar and multipolar regimes is inclined in a way that for lower electrical conductivity fluids (i.e. smaller  $Pm$ ) the dynamo tends toward the reversing regime. We speculate that

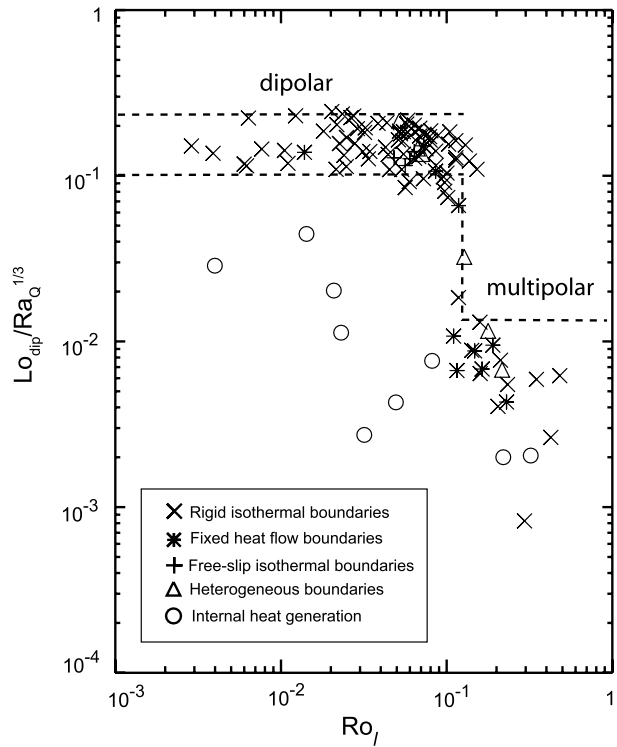
the Lorentz force stabilizes the dynamo, since larger  $Pm$  yields stronger magnetic fields and therefore stronger Lorentz forces.

This regime scenario is found at different  $E$  with some modifications. When rotation is faster, i.e. smaller  $E$ , the flow tends to obey more severely the Taylor-Proudman constraint and is organized in coherent quasi 2D axial convective columns, resulting in reduced dynamo variability and a stronger dipolar magnetic field. Therefore decreasing  $E$  allows obtaining stable dipolar dynamos with relatively larger flow magnitudes and smaller  $Pm$  values. This basically reflects a competition between Coriolis and non-linear inertial forces (Christensen and Aubert 2006). We note that reversing dynamos were obtained for rather low  $E \sim O(10^{-5})$  using appropriately large enough  $Ra$  (Takahashi et al. 2005).

The dependence of magnetic reversibility on the dynamo parameters was quantified by Christensen and Aubert (2006). They argued that the stability of the magnetic dipole depends on the local Rossby number ( $Ro_\ell$ ), which can be interpreted as a measure for the relative importance of the non-linear inertial forces. Figure 7 shows the dimensionless dipole moment  $Lo_{dip}$  normalized by the buoyancy flux-based Rayleigh number  $Ra_Q^*$  (which represents the convective power) for a large set of dynamo models. Christensen and Aubert (2006) found for dipole-dominated dynamos  $Lo_{dip} \propto Ra_Q^{*1/3}$ . A critical value of  $Ro_\ell \simeq 0.1$  in Fig. 7 marks a sharp transition from stable dipolar to reversing dynamos. This transition becomes even sharper for smaller  $E$  values (Wicht et al. 2009). The importance of  $Ro_\ell$  in determining the regime boundary indicates that non-linear inertial forces not only play a role in destroying the dipole dominance but also in facilitating reversals. Olson and Christensen (2006) fitted a power law for  $Ro_\ell$  in terms of the dynamo control parameters. The positive power of  $Ra$  and the negative powers of  $E$  and  $Pm$  confirm the qualitative interpretation of Fig. 6.

The type of convection also affects the chances of a dynamo model to reverse. Convection in Earth's outer core is driven thermally due to secular cooling and latent heat release at the inner-core boundary and chemically due to light elements release as the inner core freezes (e.g. Nimmo 2007). Figure 7 reveals an important difference between dynamos driven by volumetric heat sources in order to model secular cooling (open circles) and those driven by buoyancy flux from the inner boundary (other symbols), with the former generally less dipolar so that the transition between the dipolar to multipolar regime is more gradual. Kutzner and Christensen (2002) studied dynamos with different buoyancy boundary conditions and volumetric sources and sinks, corresponding to various scenarios of thermochemical convection, for example zero CMB buoyancy flux corresponds to chemical convection (Fig. 8). They found that the transition between dipolar to multipolar dynamos occurs at different  $Ra$  values depending on the type of convection. For example, for a given  $E$  and  $Pm$ , chemical convection requires the strongest  $Ra$  in order to obtain reversals, while either fixed flux at both boundaries or fixed temperature at both boundaries require the weakest  $Ra$ . Aubert et al. (2009) suggested that volumetric heating may also yield strongly dipolar dynamos. Hori et al. (2010) showed that fixed heat flux outer boundary condition (which is geophysically more relevant) favors dipolar dynamos, whereas fixed buoyancy favors reversing dynamos. Kutzner and Christensen (2000) demonstrated that the threshold  $Ra$  value for the transition to multipolar dynamos depends on the heating mode and on the thermal boundary conditions. In contrast, the transition seems to occur in most cases approximately around a critical local Rossby number of  $\approx 0.1$  which thus seems to be the more appropriate parameter for determining the dynamo regime. Aubert et al. (2009), however, showed that the transitional  $Ro_\ell$  weakly depends on the inner core radius.

**Fig. 7** Dimensionless dipole moment normalized by buoyancy flux-based Rayleigh number  $Lo_{dip}/Ra_Q^{1/3}$  as a function of the local Rossby number  $Ro_\ell$ , representing the transition from dipolar to multipolar dynamo models (Olson and Christensen 2006). Different symbols denote various convection types (see legend)



### 3.3 On the Quest for Dipolar Reversing Dynamos

The studies described above have set the framework within which reversals may be studied using numerical dynamos, but have also led to a somewhat disturbing result—dipole-dominated dynamos generally do not co-exist with reversing dynamos. It is important to keep in mind that the reversal phenomenon is intriguing because the geomagnetic field during chrons is strongly dominated by its axial dipole component, so reversal of the dipole means that the new field is approximately opposite to the old one, which is a drastic change. If the dipole during chrons is small compared to the total field, a reversal of the dipole may be regarded as a minor SV event. It is therefore an important challenge to find a reversing dynamo model that its relative dipole part during chrons is comparable to that of the geomagnetic field.

The dipolarity of the magnetic field is usually defined by the relative strength of the dipole at the CMB as follows:

$$d = \frac{B_d}{B_o} \tag{16}$$

where  $B_d$  is the rms dipole field, and  $B_o$  is the rms total field usually truncated at spherical harmonic degree  $\ell \sim 12\text{--}14$  to facilitate comparison with the accessible large-scale part of the observed geomagnetic field. In most studies the time-average value of  $d$  is reported. For the present geomagnetic field  $d = 0.64$  (Stacey 1992). Non-reversing numerical dynamo models obtained with low  $Ra$  may reach very large typical dipolarity values of  $d = 0.8\text{--}0.9$  (Christensen et al. 1999; Christensen and Aubert 2006). However, considerably smaller  $d$

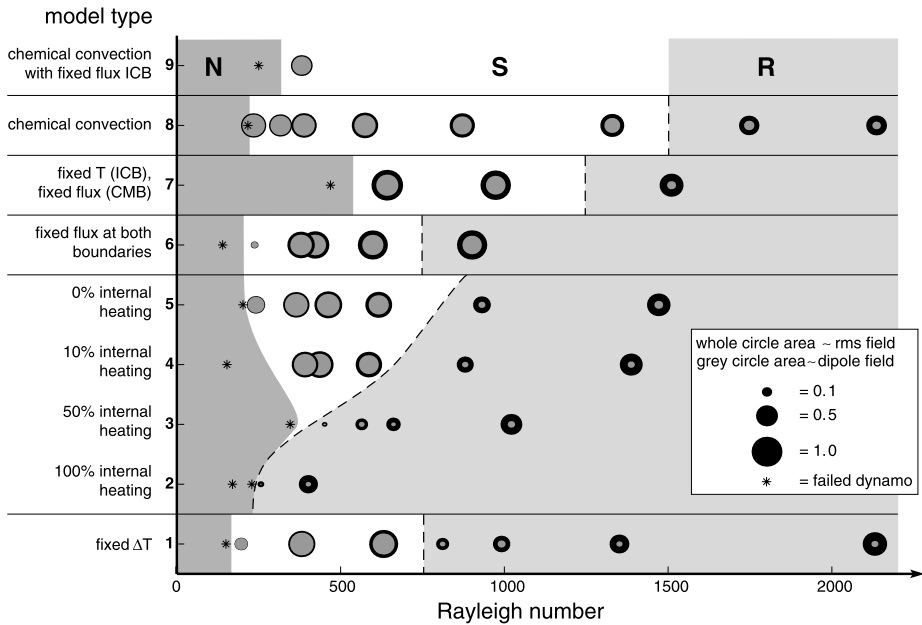


**Fig. 8** Stable dipolar and reversing multipolar regimes for different convection types as a function of  $Ra$  (Kutzner and Christensen 2002). In all case  $E = 3 \cdot 10^{-4}$ ,  $Pr = 1$  and  $Pm = 3$ . The regime of no dynamo is denoted by N, stable dynamos by S and reversing dynamos by R

values were reported for reversing dynamo models, for example  $d = 0.1-0.25$  (Kutzner and Christensen 2002),  $d = 0.4$  (Wicht 2005),  $d = 0.23-0.35$  (Aubert et al. 2008b) and  $d = 0.2-0.4$  (Wicht et al. 2010).

Probably the highest dipolarities reported for reversing dynamos were obtained by Olson (2007) using a chemical convection model with large  $E = 6.5 \times 10^{-3}$  and  $Pm = 20$  values. In the transition from non-reversing to reversing dynamos he obtained for an optimal  $Ra$  value dipolarities of  $d > 0.6$ , which gradually decrease with further increase in  $Ra$ . One of these chemical models was studied in details by Olson et al. (2009). They report a time-average and standard deviation of  $d = 0.55 \pm 0.12$ , so at some periods their model dipolarity surpasses the dipolarity of the present geomagnetic field.

As stated in the previous section, the governing parameter for the transition from dipolar to multipolar dynamos is the local Rossby number  $Ro_\ell$ . Wicht et al. (2009) point out that the left boundary of the reversing regime is hard to pin down, because the reversal likelihood decreases with  $Ro_\ell$ , and therefore dynamos might erroneously be categorized as non reversing simply because they have not yet reversed in the simulated time span. In dynamos with very large  $Ro_\ell$ , the dipole is always weak and changes its polarity on comparable time scales as the other multipoles. More Earth-like reversing dynamos with  $Ro_\ell \sim 0.1$  have a stronger dipole during stable polarity periods and a weak dipole during the rare reversals. The main challenge is therefore to understand why in the more Earth-like dynamos the dipole weakens, and why do these events occur so rarely and irregularly.

### 3.4 Reversal Frequency and Duration

So far we discussed the conditions to obtain a reversing dynamo and the level of dipolarity of those models. Another important observational constraint is the time scales involved in the

reversal process. Paleomagnetic records suggest that reversals last several kyrs, while chrons are typically much longer, on the order of several 100 kyrs. Also, the reversal frequency is time-dependent, providing another, even longer, time scale (Merrill et al. 1998). To be considered Earth-like, numerical dynamo models should capture these time scale disparities.

Long stable polarity chrons interrupted by rare reversals can be found at the transition from the dipolar to the multipolar regime for  $Ro_\ell = 0.1$  (Kutzner and Christensen 2002; Christensen and Aubert 2006). Christensen and Aubert (2006) predicted  $Ro_\ell \sim 0.09$  for Earth's core which nicely agrees with the regime where rare reversals are found. This value is based on a scaling law derived from a suit of dynamo simulations that ties  $Ro_\ell$  to the heat flux through the outer boundary, which can reasonably well be estimated for Earth. Note, however, that Earth's estimated local Rossby number  $Ro_\ell \sim 0.09$  is much smaller than estimates of the conventional Rossby number (e.g. Olsen and Mandaia 2008), requiring either core flow much stronger than that inferred from the geomagnetic secular variation, or very small length scales corresponding to  $\ell \sim 100$ . It is difficult to conceive that flows on such a small scale can significantly influence the dynamo process, let alone its reversal behavior (Wicht and Tilgner 2010). Moreover, the reason for the remarkable coincidence between the estimated  $Ro_\ell$  for Earth's core and the critical value for the transition in numerical dynamos is not clear. Finally, some dynamo models violate the critical  $Ro_\ell \sim 0.09$  reversal threshold, e.g. case C, the model of Wicht (2005), and dynamo models at large Prandtl numbers (U. Christensen, personal communication).

It is still under debate whether the variability in Earth's reversal frequency is simply due to the stochastic nature of the dynamo process (Jonkers 2003; Ryan and Sarson 2007) or also due to changes in dynamo conditions over time. The time scale associated with the reversal frequency rate of change, for example the length of the Cretaceous Normal Super Chron, is comparable to the time scale of mantle convection overturn, about ten Myrs, suggestive that changes in reversal frequency may be related to changes in CMB heat flux (Glatzmaier et al. 1999; Kutzner and Christensen 2004). Lower mantle anomalies in seismic shear wave velocity (e.g. Masters et al. 2000) have been used to impose heterogeneous heat flux pattern across the CMB (Glatzmaier et al. 1999; Coe et al. 2000; Olson and Christensen 2002; Christensen and Olson 2003; Kutzner and Christensen 2004; Gubbins et al. 2007; Willis et al. 2007; Aubert et al. 2008a; Olson et al. 2010). Glatzmaier et al. (1999) examined the impact of various imposed outer boundary heat flux patterns on the reversal frequency of their dynamo models. They found that the reversal frequency may vary substantially, including some boundary condition patterns that completely suppress reversals (Fig. 9). They argued that an imposed heat flux pattern that is compatible with the underlying convection promotes dynamo stability. They also found that increased polar heat flux that yields stronger convective plumes inside the TC produces stronger toroidal fields, leading to a larger dipole field which is less prone to reversals (Glatzmaier and Roberts 1997). In contrast, other studies argued that a positive heat flux anomaly at the equatorial region promotes stronger columnar convection outside the TC, probably leading to larger  $Ro_\ell$  values which in turn may increase the reversal likelihood (Kutzner and Christensen 2004; Olson et al. 2010). However, simple parameterized models (Ryan and Sarson 2007) and dynamo simulations (Wicht et al. 2009) seem capable of showing rather Earth-like variations in reversal frequency without evoking any changes in the CMB heat flux. Figure 10 illustrates an example of such variability in the dynamo model T4 of Wicht et al. (2009).

When trying to compare absolute time scales in the numerical simulations and the geodynamo, the dimensionless numerical results have to be rescaled. Typically, an Earth-like magnetic diffusion time  $\tau_\lambda = D^2/\lambda$  is assumed. However, in several reversing dynamo models the magnetic Reynolds number is sometimes lower than the geomagnetic value of  $Rm \sim 500$ .

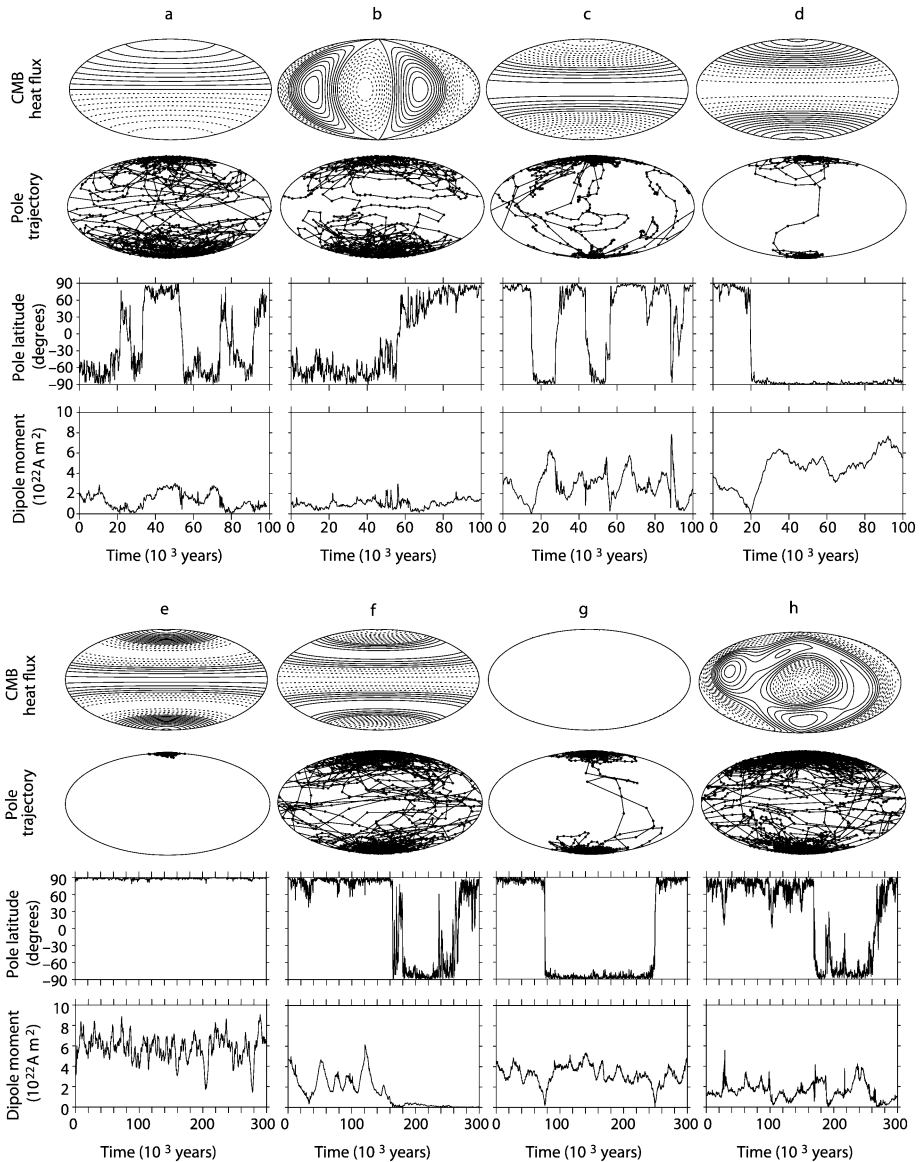


**Fig. 9** Dependence of reversal frequency on imposed outer boundary heat flux pattern (Glatzmaier et al. 1999)

Since  $Rm$  represents the ratio of magnetic diffusion time to advection time, the convective flow would be somewhat slow for these cases, which may also affect the reversal dynamics (Wicht 2005).

Most studies of reversing dynamos display quite Earth-like dipole tilt timeseries of long chrons interrupted by short reversals with irregular frequency (Glatzmaier et al. 1999; Kutzner and Christensen 2002, 2004; Wicht 2005; Olson 2007; Aubert et al. 2008b; Olson et al. 2009; Wicht et al. 2009), for example see Fig. 10. The existence of well-defined

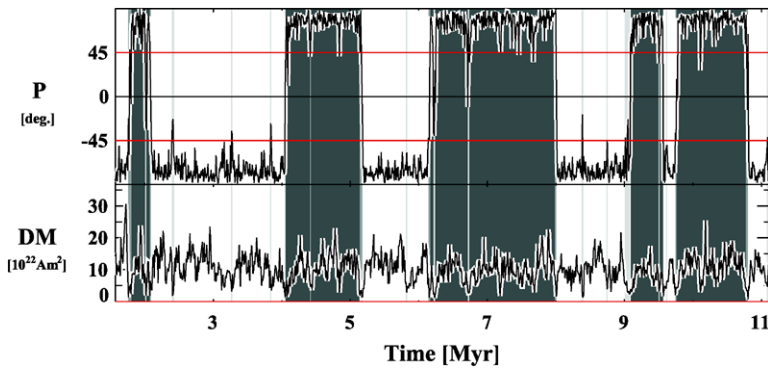


**Fig. 10** Reversal sequence for the dynamo model T4 of Wicht et al. (2009)

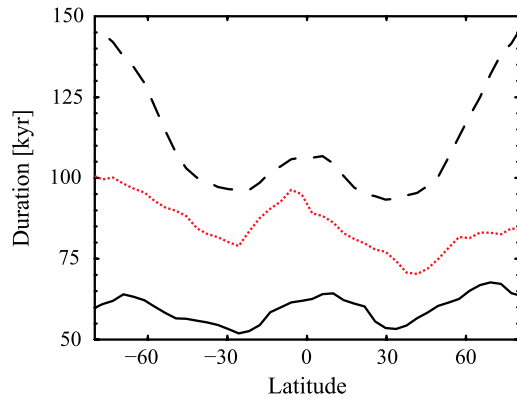
long periods of normal and inverse stable modes separated by rapid reversals was illustrated in histograms of the axial dipole that are characterized by a bimodal distribution (Aubert et al. 2008b; Olson et al. 2009). Given the uncertainties in re-scaling the simulations to real time, the durations of chrons and reversals also seem reasonably Earth-like (Wicht 2005; Olson et al. 2009). Reversal frequencies in the order of one to two per Myr and reversal duration in the order of 10 kyr have been reported, in agreement with paleomagnetic data (Merrill et al. 1998). For example, Olson et al. (2009) obtained an average of 1 Myr for the chrons duration, about twice the average chron duration for the sea floor record, and 10 kyr for the reversals duration.

The durations of geomagnetic and simulated reversals also show very similar latitudinal dependences (Clement 2004; Wicht 2005; Wicht et al. 2009) with shorter durations at the equator and a gradual increase towards the poles. Figure 11 demonstrates latitudinal site dependence in dynamo model T4 (see Table 1). Generally it is unclear whether excursions that happen right after or before a reversal are expressions of the same internal process. To clearly separate the internal processes, Wicht et al. (2009) demand that a reversal should be bracketed by a stable period of duration  $T_s$  without excursions. Figure 11 shows results for  $T_s = 10$  kyr and  $T_s = 30$  kyr. Reversals consistently last longer at higher latitudes, but also around the equator, which can be attributed to the reversed CMB flux patches typically appearing at low-latitudes (Wicht 2005; Wicht et al. 2009). Naturally, the inferred reversal duration also depends on the longitude of the site (Clement and Kent 1991; Wicht 2005; Wicht et al. 2009), although paleomagnetic records typically lack the resolution to observe this dependence (Clement and Kent 1991).

### 3.5 Field Evolution During a Reversal

In the previous sections we described the main observational constraints for modeling Earth-like reversals. We now proceed to review the time-evolution of the magnetic field during reversals obtained in numerical dynamos. Several extreme scenarios may be considered for the field evolution during a reversal. For the dipole field, one extreme scenario may involve dipole collapse until a certain minimum followed by a built up of the positive dipole axis in the other hemisphere. In another extreme scenario the dipole rotates from one hemisphere to the other without any change in the total dipole energy, just transfer of energy from the axial dipole to its equatorial part and back to the axial. The non-dipole field may decrease and recover in phase with the dipole collapse, or actually grow throughout the reversal, or

**Fig. 11** Latitudinal site dependence of inferred reversal duration for model T4 of Wicht et al. (2009) with different definitions of the critical length of bounding chrons. The *solid* and *dotted* curves show the duration estimate for a reversal assuming  $T_S = 10$  kyr and  $T_S = 30$  kyr, respectively. The *dashed* curve is an average over 15 reversals for  $T_S = 30$  kyr



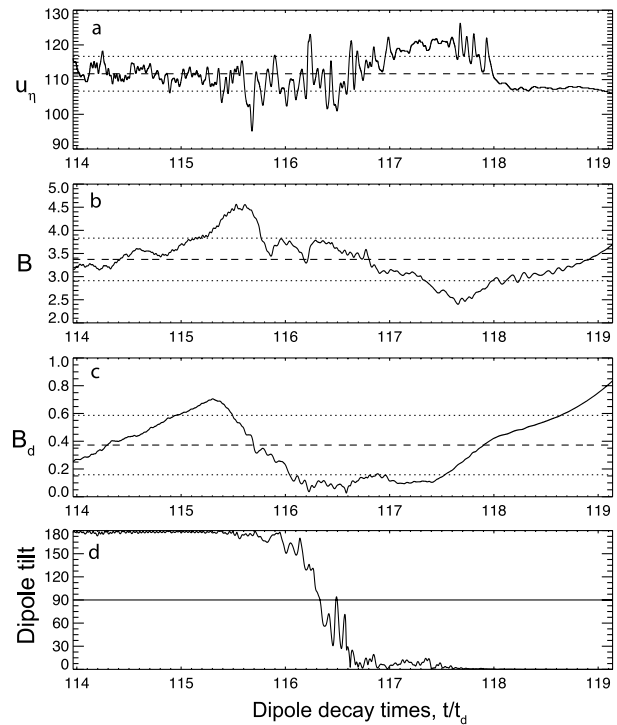
remain unchanged. Non-dipole increase during dipole collapse may be due to energy transfer from the dipole to the higher harmonics, or a dynamo configuration that favors generation of non-dipole field. We will try to identify characteristics of these scenarios in the transition fields of numerical dynamo reversals.

Reversals in most dynamo models are associated with a prolonged period of dipole collapse followed by a shorter directional instability. Olson et al. (2009) (case C in Table 1) found that dipole collapse begins about when the amplitude of flow fluctuations increases ( $t \sim 115.4$  in Fig. 12), while the rms field decreases shortly after ( $t \sim 115.7$ ). The dipole never vanishes during the reversal, indicating a significant equatorial dipole—at the height of the reversal the equatorial dipole reaches about 25% of the axial dipole prior to the reversal. The time-evolution of the dipole tilt is not monotonic, with short episodes of tilt decrease at the early stages of the reversal, as well as several equator crossings at its height when the dipole is weak and the tilt is strongly time-dependent. The recovery phase is characterized by low amplitude flow fluctuations (Fig. 12a). The outer surface radial field  $B_r$  is dominated by the axial dipole with high-latitude flux patches at the edge of the TC (Fig. 13) maintained by surface downwelling associated with deep axial cyclones. At the beginning of the reversal ( $t = 115.5$ ) the axial magnetic field  $B_z$  in the equatorial plane shows two prominent opposite-sign flux patches, with the more intense dictating the overall polarity. These two flux patches compete for control, and when they reach equal strength, the reversal takes place. In contrast, after the reversal ( $t = 119$ ) two same-sign  $B_z$  patches appear. During the dipole collapse a forward magnetic energy cascade is seen in the form of energy peaks traveling progressively from the dipole to  $l = 3$ , then to  $l = 4$  and finally to  $l = 6$  (for a more quantitative interpretation see Amit and Olson 2010), as opposed to no apparent cascade during the recovery (Fig. 14).

The reversal displayed in Figs. 12–14 contains some elements of the extreme scenarios mentioned above. Both the total field and the dipole decrease, but not in phase, and the dipole never vanishes. The equatorial dipole increases as the axial dipole decreases, but the total dipole clearly weakens, in contrast to pure dipole rotation. Dipole collapse appears before the field decrease, and forward energy cascade from the dipole to higher harmonics is observed. During the reversal the field is dominated by higher harmonics, especially  $l = 4$ . In the recovery phase the  $l = 4$  energy fades, and the dipole as well as  $l = 3$  gradually grow (Olson et al. 2009).

Wicht et al. (2009) analyzed a typical reversal in their numerical dynamo model (case T4 in Table 1). The decrease and subsequent recovery of the axial dipole contribution constitutes the main magnetic energy variations at the CMB (Fig. 15). The variation in the

**Fig. 12** Time-series of the rms flow (a), rms field (b), dipole field (c) and dipole tilt (d) during a reversal in a numerical dynamo (Olson et al. 2009). Dashed lines are time-averages, dotted denote standard deviations



other magnetic field components is very similar to the typical variation during stable polarity epochs. They do not find an increased non-dipolar contribution at the beginning of the reversal. During the dipole low, the larger time dependence of the higher harmonics makes for a very variable CMB field. The dynamo seems to have lost its capability to produce a large scale coherent field, the north/south symmetry is largely lost and non-axisymmetric contributions prevail. At times, the CMB field is dominated by single strong field patch for a few thousand years (for example  $t_2$  in Fig. 16). This results in VGP clusters similar to those observed in paleomagnetic records for those sites that are located close to a prominent patch.

The behavior of the non-dipole field during a reversal varies among the dynamo models. During the reversal of Olson et al. (2009) shown in Fig. 12 the non-dipole energy increases (which they interpret as magnetic energy cascade), whereas in the model of Wicht et al. (2009) shown in Fig. 15 the non-dipole energy is rather unchanged. The reason for this difference is not clear. The models differ in their convection styles (chemical or thermal) and control parameters, resulting in different induction strength, dipole dominance and inertial impact (see Table 1). It is possible that significant non-dipole increase can be facilitated only when the dipole prior to the reversal is large enough. Alternatively, the subtle distance in parameter space of the models from the transition from stable to reversing dynamos may affect the non-dipole strength during a reversal. Naturally, it is also possible that even for the same dynamo model different reversals show different behaviors. Additional research with a more statistical approach is clearly necessary to better understand this issue.

**Fig. 13** Radial magnetic field on the outer boundary (*left*) and axial magnetic field on the equatorial plane (*right*) before (*top*,  $t = 115.5$ ) and after (*bottom*,  $t = 119$ ) the reversal shown in Fig. 12

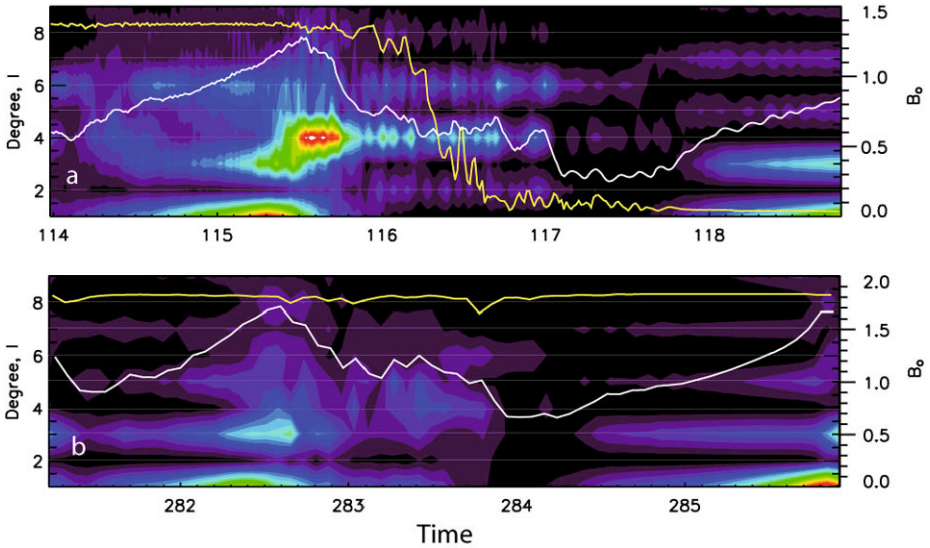
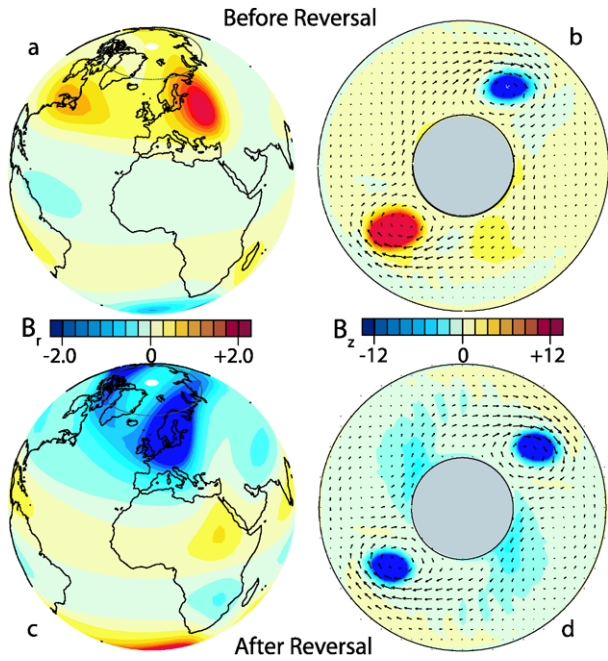


**Fig. 14** Magnetic field power spectra for a reversal (*top*) and for a dipole collapse event that did not result in a reversal (*bottom*) (Olson et al. 2009). Rms internal field (*white*, *right scale*) and dipole tilt (*yellow*) are superimposed

**Fig. 15** Time series of the dipole tilt (*top*), surface magnetic energy of the first four degrees (*middle*), and surface magnetic energy of the first four orders (*bottom*) (Wicht et al. 2009). Lines  $\ell = 1$  and  $m = 0$  are *solid*,  $\ell = 2$  and  $m = 1$  are *dotted*,  $\ell = 3$  and  $m = 2$  are *dashed*,  $\ell = 4$  and  $m = 3$  are *dash-dotted*

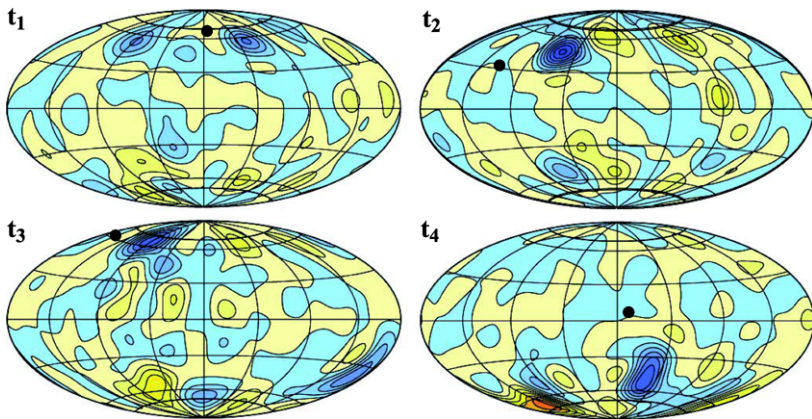
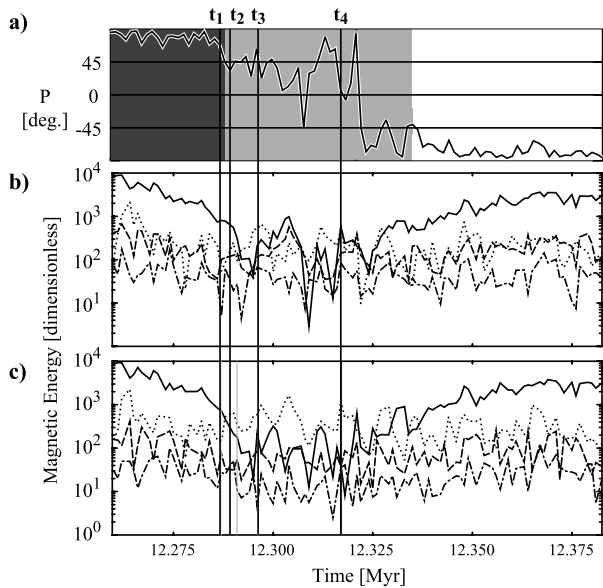


**Fig. 16** Four snapshots of the surface radial magnetic field corresponding to the times marked in Fig. 15

### 3.6 Mechanisms for Reversals and Dipole Decrease

The scenarios presented in the previous section are related to specific dynamo mechanisms. To a certain degree, the simple dipole rotation scenario is suggested since the equatorial dipole never vanishes and may even strengthen during reversals (Olson et al. 2009; Wicht et al. 2009). Magnetic energy cascade corresponds to advective (rather than diffusive) dominance in the temporal evolution of the magnetic spectrum, and is viewed as progressive traveling peaks from the dipole to higher harmonics in the magnetic field spectrum (Amit and Olson 2010). If radial diffusion is dominant, as is the case at the moment when flux is expelled from the interior of the core to the CMB (Bloxham 1986), then the dipole decrease

is expected to coincide with or followed by an abrupt increase in some high wavenumber spectral mode. The forward magnetic energy cascade is therefore a more complex advective phenomenon involving various spatial scales (Olson et al. 2009).

Several authors have observed that numerical reversals coincide with an increased equatorially symmetric magnetic field contribution (Li et al. 2002; Takahashi et al. 2005, 2007; Nishikawa and Kusano 2008; Olson et al. 2009). This is typically accompanied by an increase of the equatorially asymmetric flow which is required to convert equatorially asymmetric magnetic field into its symmetric counterpart. However, significant violations of either symmetry can already be observed for dynamos that never seem to reverse (Wicht et al. 2009). The breaking of equatorial and azimuthal symmetries is thus a necessary but not sufficient condition for reversals to occur.

To efficiently annihilate the existing dipole field on the CMB and thereby initiate a reversal, reversed radial magnetic field must be generated, expelled to the outer surface, and reach high-latitudes to replace the prevailing polarity flux. Observed emergence and growth of reversed flux on the CMB (Bloxham and Gubbins 1986; Chulliat and Olsen 2010) has been interpreted as a major cause for the decrease in the historical geomagnetic dipole moment (Cox 1975; Gubbins 1987; Olson and Amit 2006). Reversed flux patches also appear in the early stage of the paleomagnetic model for the Matuyama-Brunhes reversal (Leonhardt and Fabian 2007). Common to most reversal simulations is the importance of reversed flux patches at low- to mid-latitudes in the beginning phase of the reversal (Wicht and Olson 2004; Aubert et al. 2008b; Driscoll and Olson 2009; Olson et al. 2009). Sarson and Jones (1999) argued that fluctuations in the meridional circulation in the form of abrupt fluid upwellings originating from the inner core boundary trigger reversals. Aubert et al. (2008b) have identified distinct magnetic features tied to flow upwellings (which they termed ‘magnetic upwellings’) that advect, amplify and stretch magnetic field lines, while the bent field lines impinge the CMB to produce reversed flux patches (Wicht and Olson 2004). Equatorial upwelling plumes rising from the inner-core boundary outside the TC were also found to be pronounced reversal triggers by Rotvig (2009). Magnetic upwellings fall into two distinct categories: those that rise inside the TC and those that appear at low- to mid-latitudes. The geomagnetic field at the CMB shows reversed flux patches in both these regions (Jackson et al. 2000).

Inside the TC, magnetic upwellings are connected to convective plumes (Aurnou et al. 2003; Aubert et al. 2008b). Sreenivasan and Jones (2006) showed that fewer but thicker plumes appear in the presence of stronger background magnetic field. The plumes inside the TC can significantly reduce the background dipole field, but can tilt it only to a limited extent. More significant for reversals, however, are the low- to mid-latitude magnetic upwellings. Equatorial upwelling flows produce a large amount of reversed flux even in very simple dynamo models that never reverse. Reversed field of both polarities is produced at either side of the equatorial plane so that the effects largely cancel. In magnetic upwellings, however, the north/south coherence is obviously violated and reversed field is produced predominantly on one side of the equator (Wicht and Olson 2004; Aubert et al. 2008b; Wicht et al. 2009). This corresponds to the loss of equatorial anti-symmetry in the magnetic field and of equatorial symmetry in the flow (Li et al. 2002; Coe and Glatzmaier 2006; Takahashi et al. 2007; Nishikawa and Kusano 2008). Figure 17 shows two reversed flux patches produced by magnetic upwelling at low-latitudes in case T (see Table 1).

Aubert et al. (2008b) illustrated the line of events that lead to a reversal (Fig. 18). They identified two magnetic upwellings bringing a significant amount of reversed flux from the equatorial inner boundary toward the outer surface, where magnetic anti-cyclones stretch and amplify the field lines. Reversed flux patches appear on the outer boundary when the

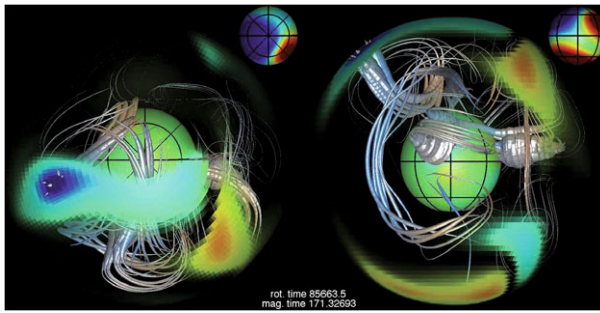


**Fig. 17** Magnetic field lines during a reversal visualized with the DMFI tool (Aubert et al. 2008b). The thickness of the field lines has been scaled with the local magnetic energy. North-polar and side view are shown at left and right, respectively. The inner core is represented by the central sphere. Color coded radial magnetic field is shown on the inner core, the outer boundary (only dominant field patches), and at a level representing Earth's surface in the upper right corner of both panels. The snapshot depicts two magnetic upwellings in the northern hemisphere that have already created enough reversed field to significantly tilt the dipole. A magnetic anticyclone can be seen in the left hemisphere

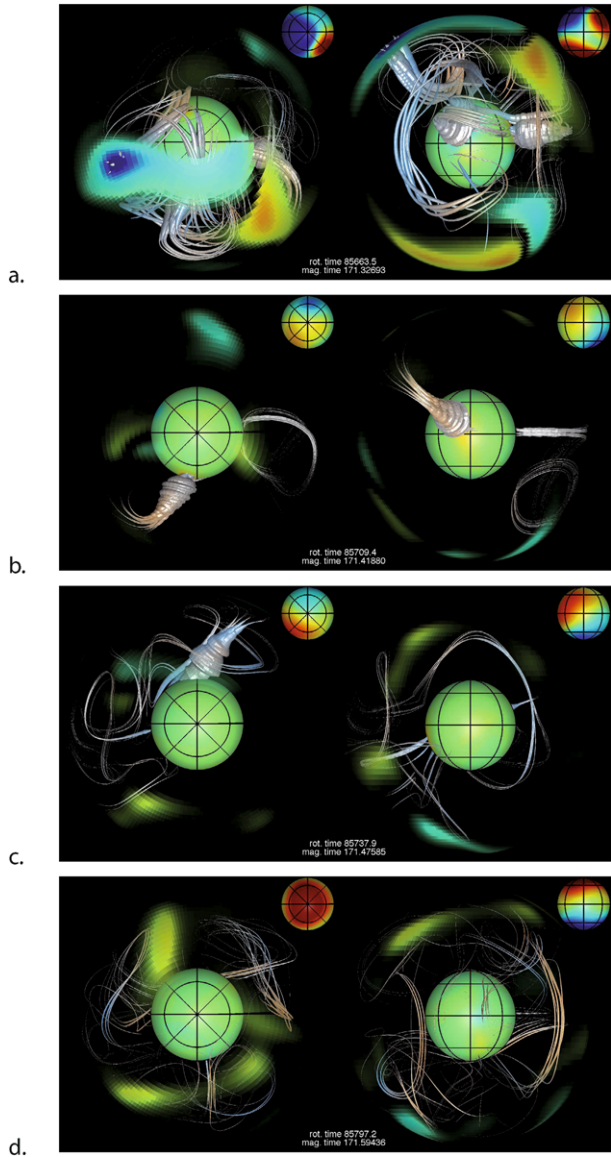
stretched field lines impinge the surface. This reversed field is subsequently advected poleward and cancels the normal polarity field to complete the reversal process.

Takahashi et al. (2005) identified similar reversal dynamics in dynamo models with much lower  $E$  values. They argued that the poleward motion of low-latitudes reversed flux patches pushes the high-latitudes normal polarity patches to the polar regions where these structures are dispersed. When the reversed flux reaches high-latitudes, strong flux patches of the new normal polarity are formed, and the reversal is terminated.

The typical time scale of the magnetic upwellings is about one kyr, but their duration, amplitude, and frequency may vary stochastically (Wicht et al. 2009). Weak magnetic field excursions can be caused by one magnetic upwelling of average amplitude. Full polarity reversals require a fierce and long lasting upwelling to sufficiently cancel the normal polarity field. Alternatively, several upwellings can team up to perform the job. Both scenarios are unlikely which explains the rareness of these events. Once the magnetic upwellings have ceased, a subsequent restart of the 'normal' dynamo mechanism may produce field of either polarity, rendering the event a reversal or an excursion (Kutzner and Christensen 2002).

Busse and Simitev (2008) describe a completely different reversal scenario based on a Parker dynamo wave: reversed flux patches emerge on either side of the equatorial plane and propagate poleward (Parker 1955; Simitev and Busse 2005). A Parker wave is a purely kinematic, linear oscillatory process that does not rely on any flow changes. Busse and Simitev (2008) find quasi oscillatory reversals in the toroidal magnetic field while the poloidal field varies much less. Only occasionally are the oscillations strong enough to cause a reversal. This explains their rareness in comparison to the proposed Parker wave period of 40 kyrs for Earth. The dynamo models of Busse and Simitev (2008) rely on differential rotation to generate the toroidal field in an  $\Omega$ -effect which is promoted by stress-free boundaries that lead to strong zonal flows. In contrast, most other reversing numerical dynamo models use rigid boundary conditions and the toroidal field is predominantly generated by an  $\alpha$ -effect (e.g. Kutzner and Christensen 2004; Wicht 2005; Aubert et al. 2008b; Olson et al. 2009; Wicht et al. 2009). Any oscillatory behavior is typically lost when the Rayleigh number is increased and the dynamics becomes more complex, as expected for Earth's core. It is therefore questionable whether the Parker-wave mechanism is meaningful for the geodynamo.

**Fig. 18** 3D field lines visualization of a reversal process (Aubert et al. 2008b)



The kinematic mechanisms responsible for dipole moment changes can be formulated based on the integral definition of the dipole moment vector and Ohm's law (Moffatt 1978; Davidson 2001). The axial component of this equation in non-dimensional form is (Olson and Amit 2006; Amit and Olson 2008)

$$\dot{m}_z = -\frac{3}{2} \int \left( u_\theta \sin\theta B_r + \frac{\lambda}{R} \frac{\partial(r B_\theta)}{\partial r} \sin\theta - \frac{\lambda}{R} \frac{\partial B_r}{\partial \theta} \sin\theta \right) dS \quad (17)$$

where  $m_z$  is the axial dipole,  $u_\theta$  meridional flow component,  $r$  and  $\theta$  radial and co-latitude spherical coordinates,  $B_r$  and  $B_\theta$  radial and meridional field components,  $R$  the outer

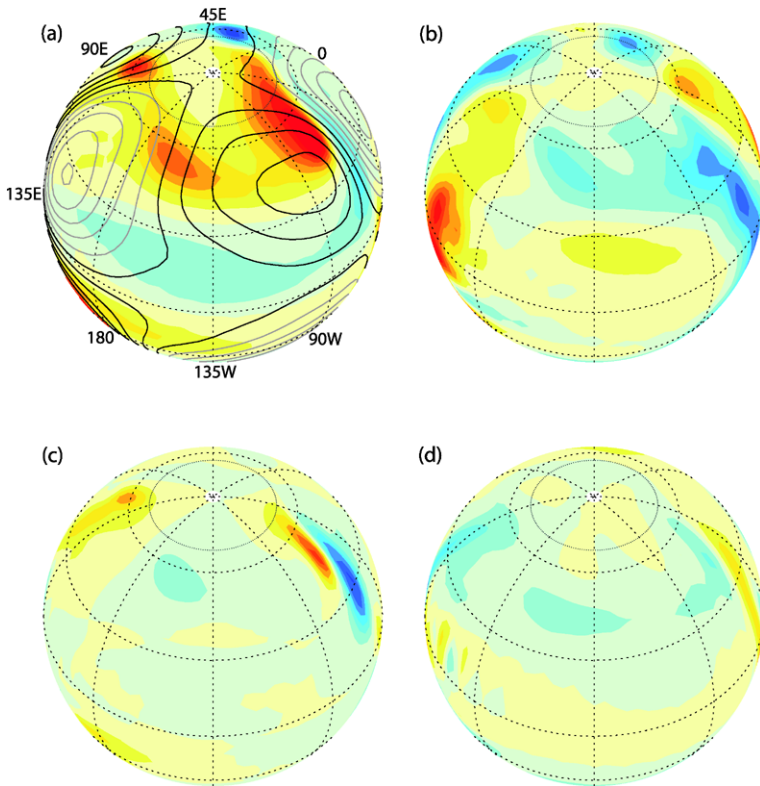


**Fig. 19** Axial Dipole Moment (ADM) change mechanisms during dipole collapse ( $t/t_d = 115.5$  in Fig. 12) (Olson et al. 2009). Radial field with streamfunction superimposed (a), radial flow (b), ADM change by meridional advection (c), and ADM change by radial diffusion (d). In (a) black/grey contours denote anti-clockwise/clockwise flow. The radial diffusion term in (d) is enhanced by a factor three with respect to the meridional advection term in (c). All images are at the top of the free stream

sphere’s radius and  $dS$  a spherical surface increment. The terms on the right hand side of (17) represent axial dipole moment (ADM) change by meridional advection, radial diffusion, and meridional diffusion, respectively.

Olson et al. (2009) applied this theory for two snapshots of a reversal. At the early stages of the reversal (Fig. 19) the field is still dominated by an axial dipole prescribed by three high-latitude intense prevailing polarity flux patches, the tilt is small, but the rate of dipole collapse is fast. The convection is organized in typical columnar structures with descending/ascending radial flows correlated with cyclones/anti-cyclones (Olson et al. 1999). Intense northward flow interacts with reversed flux at  $50^\circ\text{W}$  to yield the strongest advective ADM sink. Note that azimuthal flow produces no advective contributions to ADM change. Other advective sources and sinks due to poleward/equatorward motions of normal flux tend to cancel each other. In Fig. 20 the polarity has already reversed and the new dipole field is intensifying. No reversed flux is observed. The two new prevailing flux patches are advected poleward, producing two ADM advective sources. No advective sinks are observed. Both in the collapse and in the recovery diffusive contributions are secondary.

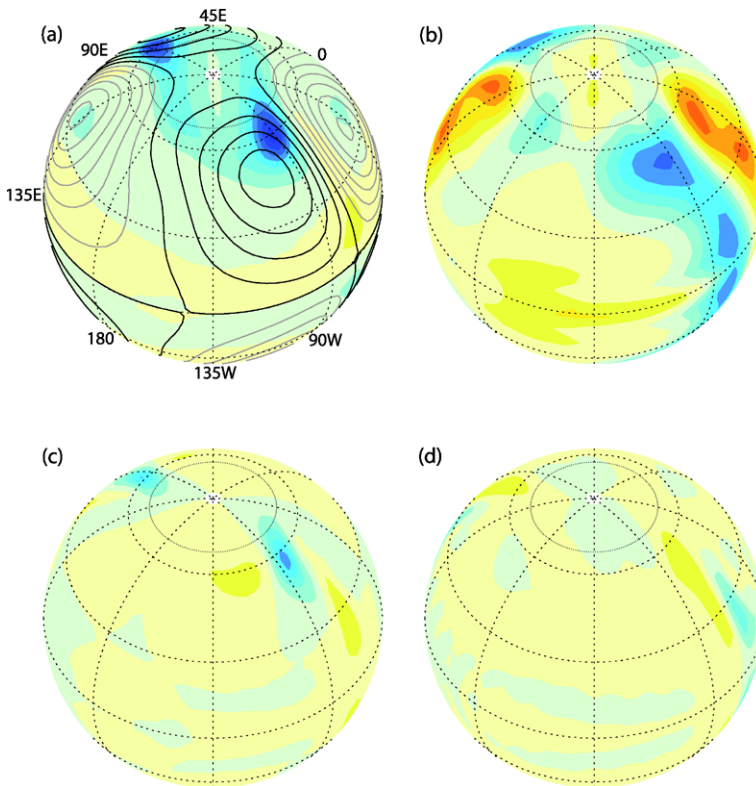


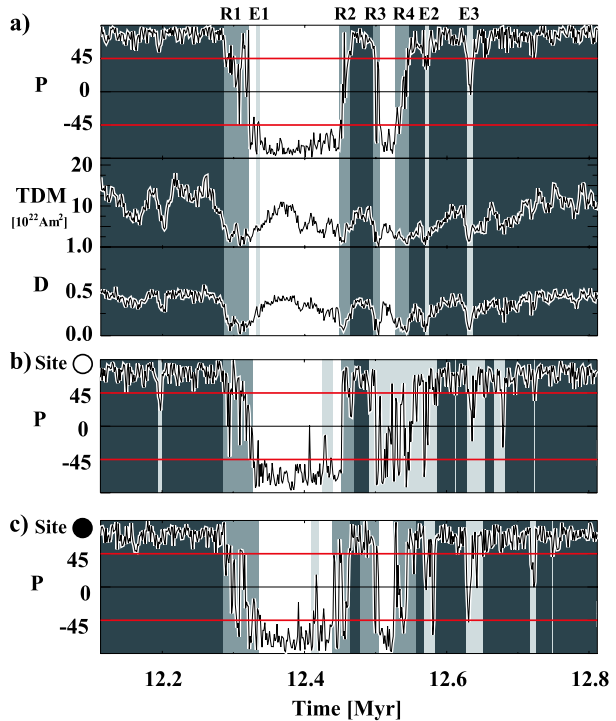
**Fig. 20** As in Fig. 19 for the recovery phase of the same reversal ( $t/t_d = 118.8$  in Fig. 12). All corresponding fields have the same contour intervals as in Fig. 19

## 4 Comparing Observations and Dynamo Models

### 4.1 Virtual Geomagnetic Poles

Most paleomagnetic analyzes of reversals and excursions rely on samples from a single site and interpretation of the directions in terms of Virtual Geomagnetic Poles (VGPs). For comparison with paleomagnetic data, several dynamo modelers have also interpreted their results in terms of VGPs. Paleomagnetic data as well as dynamo simulations suggest that the non-dipolar field contributions remain strong during reversals and excursions (Dormy et al. 2000). The VGP should therefore depend strongly on the measurement site (Glatzmaier and Roberts 1995b; Wicht 2005; Wicht et al. 2009). Figure 21 compares tilt and moment of the true dipole contribution with VGP tilt and moment from two different sites to illustrate the large site dependence. This affects estimates of excursion and reversal duration as well as the number of excursions found at a given site. Wicht et al. (2009) distinguish between local and global excursions. During global excursions the dipole decreases significantly enough that most VGPs show transitional positions during the dipole low. During local excursions the dipole decrease is milder so that the only VGPs that show transitional positions are those affected by a particularly strong flux patch on the CMB. There are also periods when the dipole becomes low without tilting significantly. Since the VGPs are influenced by the relatively strong non-dipolar field components, they are more likely to show excursive positions than the dipole itself.

**Fig. 21** True dipole (a) and VGP distributions from two sites (b and c) for a numerical dynamo model (Wicht et al. 2009)



Dynamo simulations show VGPs clustering during reversals, in agreement with several paleomagnetic models. Depending on site location, the VGP may linger for an extensive period in a limited longitude/latitude region. Paleomagnetic reconstructions of the global field (Leonhardt and Fabian 2007; Ingham and Turner 2008) indicate that the occurrence of VGP clustering or continuous paths depends on site location. In particular the position of the site relative to prominent quasi-stationary flux patches is important (Leonhardt and Fabian 2007). Based on dynamo simulations, Wicht et al. (2009) reached the same conclusion and suggested that such strong CMB flux patches can remain roughly stationary during about 1 kyr.

Some paleomagnetic studies suggest that transitional VGPs during several reversals preferentially fall into two longitude bands about  $180^\circ$  apart that roughly coincide with the areas of increased CMB heat flux in the tomographic models (Laj et al. 1991; Love 1998; Merrill and McFadden 1999). Coe et al. (2000) and Kutzner and Christensen (2004) demonstrated that the two preferred bands can be recovered in dynamo simulations when lower mantle tomographic models are used to impose a CMB heat flux pattern (see Fig. 22). Another tomographic reversal analyzed by Coe et al. (2000) does not show two longitudinal confinements but only a single band across the Pacific. The observational model IMMAB4 also suggests a Pacific preference. A possible mechanism for longitudinal preference is the increased heat flux underneath the Pacific rim that drives somewhat stronger downwellings in these regions which in turn promote the appearance of more intense magnetic flux patches of both polarities. These patches may dominate the magnetic field during reversals, thus attracting the VGPs to nearby paleomagnetic sites (Coe et al. 2000; Kutzner and Christensen 2004; Wicht et al. 2009). Equatorial dipole contributions tied to particularly strong local patches at one of the bands can be strong at times. The true dipole

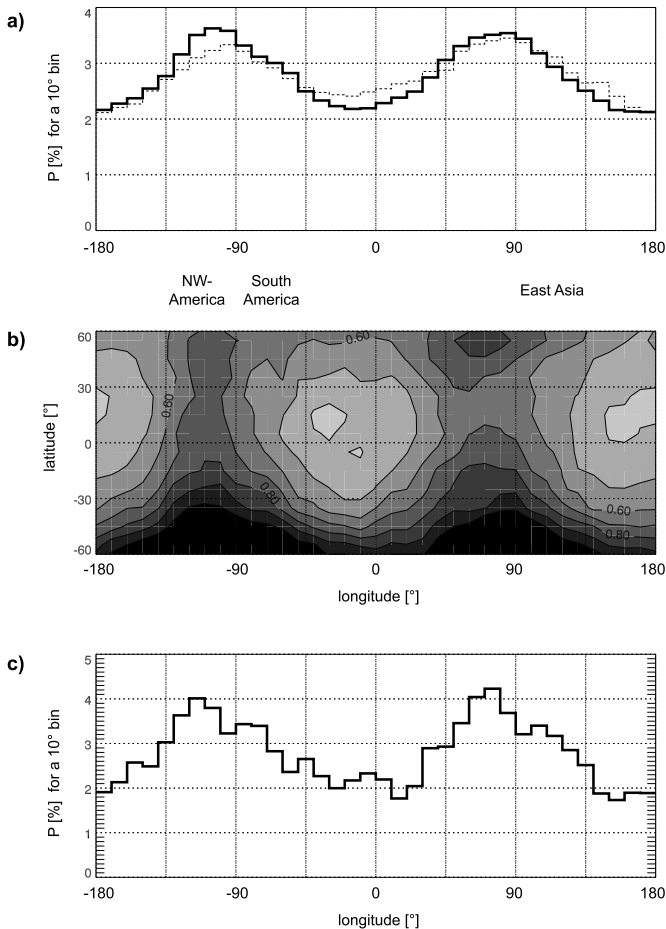


**Fig. 22** VGP distribution for a numerical dynamo with tomographic heat flux outer boundary conditions (Kutzner and Christensen 2004). (a) Probability to fall within a  $10^\circ$  bin of the strong (*solid*) and weaker (*dashed*) boundary heterogeneity, (b) VGP density map, and (c) True geomagnetic pole (TGP) probability

can thus prefer the same band as the VGPs on time average (Kutzner and Christensen 2000; Wicht et al. 2009). Remaining differences between VGP predictions of tomographic dynamo models to those of some paleomagnetic observations may be attributed to the parameter-dependence of the shift between CMB heat flux structures and thermal anomalies at the top of the core (Olson and Christensen 2002; Aubert et al. 2007; Amit et al. 2008). In addition it is worth noting that some paleomagnetic studies argue that the VGP longitudinal preferences are an artifact of data selection and weighting (Prévoit and Camps 1993; Valet and Herrero-Bervera 2003).

#### 4.2 Field Evolution During a Polarity Transition

Several significant similarities appear between the field evolution during a reversal inferred from the observations and the numerical dynamo models. Perhaps most pronouncedly, the time-evolution of the dipole is out of phase with the non-dipole field. In the observational

model, the non-dipole energy increases prior to the reversal, exceeds the dipole energy, and only later both dipole and non-dipole energies decrease simultaneously during the reversal. In the recovery phase the dipole energy increases while the non-dipole part remains weak. In many recent numerical dynamo models, the dipole collapse precedes the decrease in the total rms field. The dipole commences its recovery prior to the increase in the total field, so the dipole and non-dipole field components are once again off-phase. It is important to note that in the observational model the dipole and non-dipole energies are estimated at Earth's surface rather than on the CMB.

Both observational and numerical models find formation of low-latitude flux patches and their poleward motion during the reversal. Numerical dynamo models show that reversed flux patches are the surface expression of strong reversed field generated by plume-like flow upwellings in the depth of the outer core (Wicht and Olson 2004; Aubert et al. 2008b). The poleward motion is caused by meridional advection of the reversed flux at the top of the shell.

Observational models find significant differences in the time-evolution of the dipole and non-dipole energies when comparing the last reversal and excursion, with the non-dipole contributions being more significant in the reversal than in the excursion (Leonhardt and Fabian 2007; Leonhardt et al. 2009). Gubbins (1999) argued that a reversal will occur only if the new stable polarity will persist longer than the diffusive time scale in the inner core (about 3 kyr), whereas an excursion may take place if the field reverses in the outer core over an advective time scale (about 60 yr) but not in the inner core. However, numerical dynamo models show that the inner core plays a little role in the dynamics (Wicht 2002; Simitev and Busse 2005), so it is hard to conceive that the inner core diffusive time scale should matter. Wicht et al. (2009) argued that magnetic upwellings are often too weak or too short living to cancel the prevailing polarity. Several magnetic upwellings may team up to do the job, but this is rare, explaining why excursions are more numerous than reversals in paleomagnetic records. Once, however, the dipole is sufficiently decreased, it is a matter of chance whether it will end as a reversal or excursion (Kutzner and Christensen 2002). The numerical dynamo models of Takahashi et al. (2007) also detect different behavior between a reversal and an excursion. In both cases deep core anti-cyclones produce reversed flux that reaches the CMB at the beginning of the polarity transition. However, in the excursion the reversed flux is not generated successively and the original polarity is retrieved, whereas in the reversal the reversed flux is persistently generated at the deep core. These differences between reversals and excursions inferred from both the observational and the numerical models suggest a somewhat distinctive nature to excursions and reversals.

Some differences between the observational and numerical models are also evident. The numerical dynamo model of Olson et al. (2009) shows increase of the non-dipole field during the reversal accompanied with loss of equatorial symmetry in the flow and loss of equatorial antisymmetry in the magnetic field, while the dynamo model of Wicht et al. (2009) shows that the non-dipolar components remain unchanged. In contrast, the observational models exhibit a decrease in the non-dipole field during the reversal. Observational models predict that a reversal starts by local field reversal inside one hemisphere TC. Some reversals in numerical dynamo models also show reversed flux inside the TC (Wicht and Olson 2004; Rotvig 2009). However, in most numerical dynamo models the field inside the TC seems of minor significance for the reversal process, and the appearance of reversed flux at low- and mid-latitudes outside the TC in both hemispheres seems much more decisive.

Different behavior between dipole collapse and recovery phases is found in the saw tooth pattern of dipole strength (e.g. Valet et al. 2005) and in the dipole and non-dipole energy curves from the observational model (Leonhardt and Fabian 2007). The numerical

dynamo model of Olson et al. (2009) also shows several remarkable differences between these two phases. During the collapse, the flow exhibits high frequency fluctuations, the magnetic field has both normal and reversed flux at the CMB, the dipole change is governed by mixed advective sources and (more) sinks, and magnetic energy cascade from the dipole to higher harmonics is observed. In contrast, during the recovery the flow fluctuations are weak, no reversed flux appears on the CMB, the dipole change is governed by advective sources only, and no energy cascade is seen. However, dipole collapse and recovery are rather similar in many other dynamo simulations (Kutzner and Christensen 2004; Wicht 2005; Wicht et al. 2009), and the non-dipole remains unchanged in the model of Wicht et al. (2009). We speculate that these differences among the dynamo models are related to their level of dipolarity or to the role of inertia, though further investigation is clearly required to shed light on the origin of these discrepancies.

### 4.3 Possible Precursors?

Analysis of reversals in numerical dynamos has enabled the mechanisms responsible for these stochastic events to be dissected. However, there still remains the considerable challenge of finding whether reversals can be predicted. The geomagnetic dipole intensity in the historical era has been rapidly decreasing (Gubbins 1987; Gubbins et al. 2006), much faster than the rate of free decay in the core (Olson and Amit 2006). Moreover, the dipole axis in the past 50 years is rapidly drifting poleward after a century of maintaining a nearly steady latitude (Amit and Olson 2008). These changes could in principle signal the early stages of a reversal, although statistically most dipole collapse events in the paleomagnetic record did not end in a reversal (Valet et al. 2005). Could numerical dynamos guide us towards possible observable precursors for reversals?

Olson et al. (2009) proposed two types of reversal precursors. The first, based on scatter diagrams of dipole intensity  $m_z$  vs. its time-derivative  $\dot{m}_z$  separated to stable and reversing periods, clearly shows that the dipole reaches lower minima and maxima during reversing periods, with the lower minima being crucial as it drops below a critical level that allows reversals. The second is based on latitude-time (butterfly) plots of the axial dipole moment density  $\rho_z = B_r \cos \theta$  zonally-averaged and separated to positive and negative contributions. Comparing such plots between a dipole collapse that led to a reversal to another that produced only a minor tilt change (Fig. 23), Olson et al. (2009) found that the ratio of positive/negative zonal  $\rho_z$  at a time when the dipole axis is very close to the geographical pole is significantly larger in the reversing case. An intermediate value of this ratio can therefore serve as a reversal precursor, at least for this dynamo model. We note that a more meaningful statistics is required in order to confirm the existence of such a reversal precursor.

Could these precursors be applied to the Earth? The butterfly plot for the present geomagnetic field shows that the ratio of positive to negative zonal  $\rho_z$  is below the ratio for the non-reversing dipole collapse (Olson et al. 2009), suggesting that the current geomagnetic dipole decrease does not indicate an upcoming reversal at the moment. The same conclusion has been drawn from paleomagnetic reconstructions. When comparing the trends and ratios of the dipolar and non-dipolar contributions to modern data, a clear tendency towards an imminent excursion or reversal is not apparent (Leonhardt et al. 2009).

Hulot et al. (2010) studied growth rates of perturbations in numerical dynamos over a broad range of parameters. They claimed that the magnetic Reynolds number  $Rm$  determines the dynamo memory time. Extrapolating to the Earth, they concluded that predictions are not possible for more than one century. They specifically argued that the dynamo model of Olson et al. (2009) was capable of detecting reversal precursors only due to its relatively

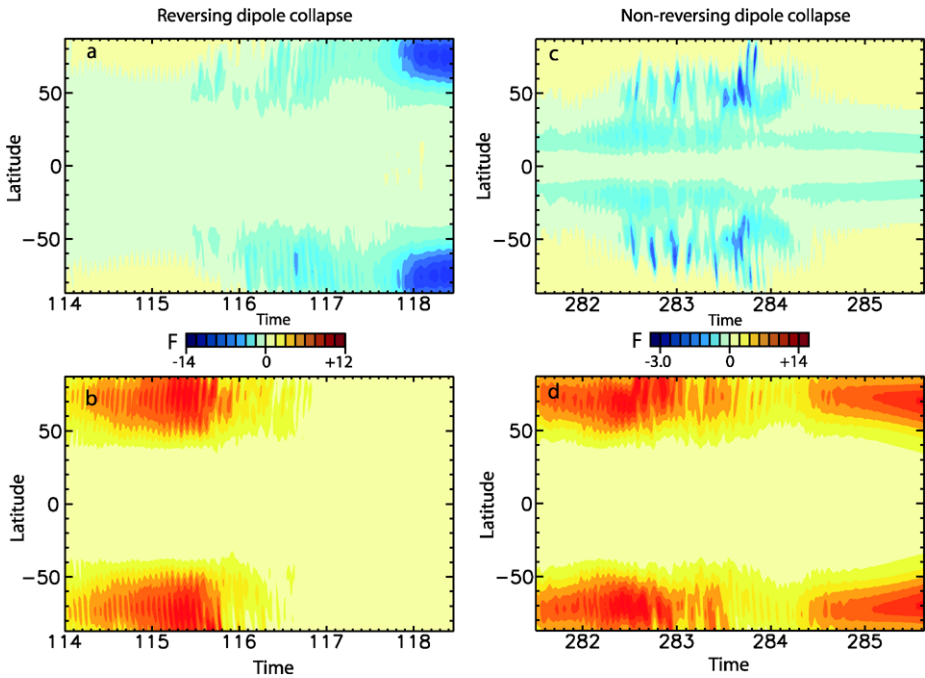


**Fig. 23** Butterfly plots of zonal axial dipole moment density separated to positive and negative contributions for the reversing (*left*) and non-reversing (*right*) dipole collapse cases (Olson et al. 2009). Note scale differences

small  $Rm$ . Nevertheless, reversed flux proliferation and the inclination of the butterfly wings indicating poleward migration of reversed flux in the present geomagnetic field on the CMB is qualitatively in agreement with early stages of dipole collapse in the numerical dynamo model of Olson et al. (2009).

## 5 Outlook

In this paper, we reviewed recent results concerning geomagnetic field polarity changes. One type of studies stems from paleomagnetic observations, the other from numerical dynamo simulations. In the observational studies, reversal duration estimates range 1–10 kyr (depending on site location). The transitional fields during the last reversal and excursion contain low-latitude reversed flux that migrate poleward. In the reversal the non-dipole field energy exceeds significantly the dipole field energy for a period of 2 kyr, whereas in the excursion the non-dipole remains at most of the period lower than the dipole. In the numerical dynamo studies, stronger convection, slower rotation, and lower electrical conductivity provide more favorable conditions for reversals to occur. Stable polarity periods typically last 1 Myr, whereas reversals last about 10 kyr. Reversals often involve prolonged dipole collapse followed by shorter directional instability. Magnetic upwellings from the equatorial inner-core boundary that produce reversed flux patches at low-latitudes of the CMB are significant in triggering reversals. Poleward advection of reversed flux and equatorward advection of normal flux dominate the field variation on the CMB during a reversal.

The time-evolution of the non-dipole field during a reversal is under debate. In the observational model of the Matuyama/Brunhes reversal the non-dipole energy decreases in phase with the dipole energy. In some numerical dynamo models the non-dipole energy remains unchanged during the dipole collapse, while in other models the non-dipole energy actually increases during the reversal and energy cascades from the dipole to higher harmonics. The possible difference between dipole collapse and recovery phases is also under debate. Observational models find asymmetry between the dipole and non-dipole energy curves in the two phases. During the collapse phase, some numerical dynamo models find both intense normal and reversed flux at the CMB, and mixed advective sources and (more) sinks of axial dipole. During the recovery phase these models exhibit very little reversed flux, and practically only advective sources. In contrast, other dynamo models do not observe significant differences between the collapse and recovery phases.

An important open question concerns the transition from stable dipolar to reversing multipolar dynamos. First, the absence of an overlap regime is problematic because the geodynamo both possesses a dipolar field during chrons and reverses occasionally. Second, while the local Rossby number seems in most cases to determine well whether a dynamo model will reverse or not, some deviations from this rule appear, e.g. in gravitational dynamos (case C) or at large Prandtl numbers (U. Christensen, personal communication). Third, it is somewhat puzzling that the geodynamo is located so close to the transition. Finally, the local Rossby number for Earth's core suggests much stronger inertial effects than commonly estimated. It therefore seems that the determination of the transition from stable to reversing dynamos should be refined. A possible step forward could be to calculate a new local Rossby number based on two length scales, one representing inertia and another (axial) measuring the Coriolis force.

Better global coverage and higher quality data are necessary in order to improve observational models of the last reversal and excursion or to apply the suggested techniques to other geomagnetic events. Especially, data is needed from the southern hemisphere and from the polar regions where currently only few records exist. Improved paleomagnetic determination and chronology techniques would provide higher confidence in the data. On the dynamo modeling side, efforts to understand the discrepancies in the interpretations of various numerical dynamo models may shed light on the robustness of some conflicting features. Systematic parametric studies with different convection styles and boundary conditions are needed to confirm the current results. For example, the more realistic prescribed heat flux boundary condition on the CMB is less studied than fixed temperatures. As computational power increases, dynamo models with smaller Ekman numbers that require higher resolution simulations may become available for studies of reversals in more Earth-like conditions. Finally, interactions between the observational, experimental and modeling communities, which do not occur often enough, may lead to unraveling the nature of geomagnetic field reversals. We hope that this paper will encourage such collaborations in the future.

**Acknowledgements** We are grateful to an anonymous reviewer for constructive comments that significantly improved the manuscript

## References

- L. Alldredge, Harmonics required in main field and secular variation models. *J. Geomagn. Geoelectr.* **36**, 63–72 (1984)
- H. Amit, P. Olson, Geomagnetic dipole tilt changes induced by core flow. *Phys. Earth Planet. Inter.* **166**, 226–238 (2008)

- H. Amit, P. Olson, A dynamo cascade interpretation of the geomagnetic dipole decrease. *Geophys. J. Int.* **181**, 1411–1427 (2010)
- H. Amit, J. Aubert, G. Hulot, P. Olson, A simple model for mantle-driven flow at the top of Earth's core. *Earth Planets Space* **60**, 845–854 (2008)
- J. Aubert, H. Amit, G. Hulot, Detecting thermal boundary control in surface flows from numerical dynamos. *Phys. Earth Planet. Inter.* **160**, 143–156 (2007)
- J. Aubert, H. Amit, G. Hulot, P. Olson, Thermo-chemical wind flows couple Earth's inner core growth to mantle heterogeneity. *Nature* **454**, 758–761 (2008a)
- J. Aubert, J. Aurnou, J. Wicht, The magnetic structure of convection-driven numerical dynamos. *Geophys. J. Int.* **172**, 945–956 (2008b)
- J. Aubert, S. Labrosse, C. Poitou, Modelling the paleo-evolution of the geodynamo. *Geophys. J. Int.* **179**, 1414–1428 (2009)
- J. Aurnou, S. Andreadis, L. Zhu, P. Olson, Experiments on convection in Earth's core tangent cylinder. *Earth Planet. Sci. Lett.* **212**, 119–134 (2003)
- S. Baumgartner, J. Beer, J. Masarik, G. Wagner, L. Meynadier, H.A. Synal, Geomagnetic modulation of the  $^{36}\text{Cl}$  flux in the grip ice core, greenland. *Science* **279**(5355), 1330–1332 (1998)
- M. Berhanu, R. Monchaux, S. Fauve, N. Mordant, F. Petrelis, A. Chiffaudel, F. Daviaud, B. Dubrulle, L. Marie, F. Ravelet, M. Bourgoin, P. Odier, J.-F. Pinton, R. Volk, Magnetic fld reversals in an experimental turbulent dynamo. *Europhys. Lett.* **77** (2007). doi:[10.1209/0295-5075/77/59001](https://doi.org/10.1209/0295-5075/77/59001)
- C.L. Blanchet, N. Thouveny, T. de Garidel-Thoron, Evidence for multiple paleomagnetic intensity lows between 30 and 50 ka bp from a western equatorial pacific sedimentary sequence. *Quat. Sci. Rev.* **25**, 1039–1052 (2006)
- U. Bleil, T.V. Dobeneck, Geomagnetic events and relative paleointensity records; clues to high-resolution paleomagnetic chronostratigraphies of late quaternary marine sediments?, in *Use of Proxies in Paleoceanography; Examples from the South Atlantic*, ed. by G. Fischer, G. Wefer (Springer, Berlin, 1999), pp. 635–654
- J. Bloxham, The expulsion of magnetic flux from the Earth's core. *Geophys. J. R. Astr. Soc.* **87**, 669–678 (1986)
- J. Bloxham, D. Gubbins, Geomagnetic field analysis—iv. Testing the frozen-flux hypothesis. *Geophys. J. R. Astr. Soc.* **84**, 139–152 (1986)
- J. Bloxham, A. Jackson, Fluid flow near the surface of the Earth's outer core. *Rev. Geophys.* **29**, 97–120 (1991)
- N. Bonhommet, J. Babkine, Sur la presence daimentations inversees dans la chaine des puy. *C. R. Acad. Sci. Ser. B* **264**, 92 (1967)
- M.B. Brown, R. Holme, A. Bargery, Exploring the influence of the non-dipole field on magnetic records for field reversals and excursions. *Geophys. J. Int.* **168**, 541–550 (2007)
- B. Brunhes, Recherches sur le direction d'aimantation des roches volcaniques. *J. Phys.* **5**, 705–724 (1906)
- F. Busse, R. Simitev, Toroidal flux oscillation as possible cause of geomagnetic excursions and reversals. *Phys. Earth Planet. Inter.* **168**, 237–243 (2008)
- S.C. Cande, D.V. Kent, Revised calibration of the geomagnetic polarity timescale forthe late cretaceous and cenozoic. *J. Geophys. Res.* **100**, 6093–6095 (1995)
- W.S. Cassata, B.S. Singer, J. Cassidy, Laschamp and mono lake geomagnetic excursions recorded in new zealand. *Earth Planet. Sci. Lett.* **268**, 76–88 (2008)
- J.E.T. Channell, Late brunhes polarity excursions (mono lake, laschamp, iceland basin and pringle falls) recorded at odp site 919 (Irminger basin). *Earth Planet. Sci. Lett.* **244**, 378–393 (2006)
- U. Christensen, J. Aubert, Scaling properties of convection-driven dynamos in rotating spherical shells and application to planetary magnetic fields. *Geophys. J. Int.* **166**, 97–114 (2006)
- U. Christensen, P. Olson, Secular variation in numerical geodynamo models with lateral variations of boundary heat flow. *Phys. Earth Planet. Inter.* **138**, 39–54 (2003)
- U. Christensen, J. Wicht, Numerical dynamo simulations, in *Treatise on Geophysics*, ed. by P. Olson, vol. 8 (Elsevier, Amsterdam, 2007)
- U. Christensen, P. Olson, G. Glatzmaier, Numerical modelling of the geodynamo: a systematic parameter study. *Geophys. J. Int.* **138**, 393–409 (1999)
- A. Chulliat, N. Olsen, Observation of magnetic diffusion in the Earth's outer core from Magsat, Ørsted and CHAMP data. *J. Geophys. Res.* **115**, B05105 (2010). doi:[10.1029/2009JB006994](https://doi.org/10.1029/2009JB006994)
- B.M. Clement, Geographical distribution of transitional VGPs: evidence for non-zonal symmetry during the matuyama-brunhes geomagnetic reversal. *Earth Planet. Sci. Lett.* **104**, 48–58 (1991)
- B.M. Clement, Dependence of the duration of geomagnetic polarity reversals on site latitude. *Nature* **428**, 637–640 (2004)
- B.M. Clement, D.V. Kent, A southern hemisphere record of the matuyama-brunhes polarity reversal. *Geophys. Res. Lett.* **18**, 81–84 (1991)

- R. Coe, G. Glatzmaier, Symmetry and stability of the geomagnetic field. *Geophys. Res. Lett.* **33**, L21311 (2006)
- R.S. Coe, L. Hongre, G.A. Glatzmaier, An examination of simulated geomagnetic reversals from a palaeomagnetic perspective. *Philos. Trans. R. Soc. Lond.* **358**, 1141–1170 (2000)
- A. Cox, Reversed flux as reversal mechanism. *Rev. Geophys. Space Phys.* **13**, 35–51 (1975)
- A. Cox, J. Hillhouse, M. Fuller, Paleomagnetic records of polarity transitions, excursions, and secular variation. *Rev. Geophys. Space Phys.* **13**, 185–189 (1975)
- P. Davidson, *An Introduction to Magnetohydrodynamics* (Cambridge University Press, Cambridge, 2001)
- E. Dormy, J.-P. Valet, V. Courtillot, Numerical models of the geodynamo and observational constraints. *Geochem. Geophys. Geosyst.* **1**(10), 1037 (2000). doi:[10.1029/2000GC000062](https://doi.org/10.1029/2000GC000062)
- P. Driscoll, P. Olson, Polarity reversals in geodynamo models with core evolution. *Earth Planet. Sci. Lett.* **282**, 24–33 (2009)
- G. Glatzmaier, Numerical simulation of stellar convective dynamos. 1: The model and method. *J. Comp. Phys.* **55**, 461–484 (1984)
- G. Glatzmaier, Dynamo models: how realistic are they? *Annu. Rev. Earth Planet. Sci.* **30**, 237–257 (2002)
- G. Glatzmaier, P. Roberts, A three-dimensional convective dynamo solution with rotating and finitely conducting inner core and mantle. *Phys. Earth Planet. Inter.* **91**, 63–75 (1995a)
- G. Glatzmaier, P. Roberts, A three-dimensional self-consistent computer simulation of a geomagnetic field reversal. *Nature* **377**, 203–209 (1995b)
- G. Glatzmaier, P. Roberts, Simulating the geodynamo. *Comput. Phys.* **38**, 269–288 (1997)
- G. Glatzmaier, R. Coe, L. Hongre, P. Roberts, The role of the earth's mantle in controlling the frequency of geomagnetic reversals. *Nature* **401**, 885–890 (1999)
- D. Gubbins, Mechanism for geomagnetic polarity reversals. *Nature* **326**, 167–169 (1987)
- D. Gubbins, The distinction between geomagnetic excursions and reversals. *Geophys. J. Int.* **137**, F1–F3 (1999)
- D. Gubbins, A. Jones, C. Finlay, Fall in Earth's magnetic field is erratic. *Science* **312**, 900–902 (2006)
- D. Gubbins, P. Willis, B. Sreenivasan, Correlation of Earth's magnetic field with lower mantle thermal and seismic structure. *Phys. Earth Planet. Inter.* **162**, 256–260 (2007)
- H. Guillou, B.S. Singer, C. Laj, C. Kissel, S. Scailleta, B.R. Jicha, On the age of the laschamp geomagnetic excursion. *Earth Planet. Sci. Lett.* **227**, 331–341 (2004)
- Y. Guyodo, J.-P. Valet, Global changes in intensity of the earth's field during the past 800 kyr. *Nature* **399**, 249–252 (1999)
- F. Heller, Self-reversal of natural remanent magnetisation in the olby-laschamp lavas. *Nature* **284**(5754), 334–335 (1980)
- K.A. Hoffman, Palaeomagnetic excursions, aborted reversals and transitional fields. *Nature* **294**, 67–69 (1981)
- K.A. Hoffman, Dipolar reversal states of the geomagnetic field and core mantle dynamics. *Nature* **359**, 789–794 (1992)
- K.A. Hoffman, Transitional paleomagnetic field behavior: Preferred paths or patches? *Surv. Geophys.* **17**, 207–211 (1996)
- K. Hori, J. Wicht, U. Christensen, The effect of thermal boundary conditions on dynamos driven by internal heating. *Phys. Earth Planet. Inter.* (2010). doi:[10.1016/j.pepi.2010.06.011](https://doi.org/10.1016/j.pepi.2010.06.011)
- G. Hulot, F. Lhuillier, J. Aubert, Earth's dynamo limit of predictability. *Geophys. Res. Lett.* **37**, L06305 (2010). doi:[10.1029/2009GL041869](https://doi.org/10.1029/2009GL041869)
- M. Hyodo, Possibility of reconstruction of the past geomagnetic field from homogeneous sediments. *J. Geomagn. Geoelectr.* **36**, 45–62 (1984)
- M. Ingham, G. Turner, Behaviour of the geomagnetic field during the matuyama-brunhes polarity transition. *Phys. Earth Planet. Inter.* **168**, 163–178 (2008)
- A. Jackson, A. Jonkers, M. Walker, Four centuries of geomagnetic secular variation from historical records. *Philos. Trans. R. Soc. Lond.* **A358**, 957–990 (2000)
- D. Jault, Axial invariance of rapidly varying diffusionless motions in the Earth's core interior. *Phys. Earth Planet. Inter.* **166**, 67–76 (2008)
- A. Jonkers, Long-range dependence in the cenozoic reversal record. *Phys. Earth Planet. Inter.* **135**, 253–266 (2003)
- C. Kissel, C. Laj, L. Labeyrie, T. Dokken, A. Voelker, D. Blamart, Rapid climatic variations during marine isotope stage 3: magnetic analyses of sediments from Nordic seas and north Atlantic. *Earth Planet. Sci. Lett.* **171**, 489–502 (1999)
- M.F. Knudsen, P.M. Holm, N. Abrahamsen, Paleomagnetic results from a reconnaissance study of Santiago (cape verde islands): Identification of cryptochron c2r.2r-1. *Phys. Earth Planet. Inter.* **173**, 279–289 (2009)

- M. Korte, C. Constable, Continuous geomagnetic field models for the past 7 millennia: 2, cal5k. *Geochem. Geophys. Geosyst.* **6**, Q02H16 (2005). doi:[10.1029/2004GC000801](https://doi.org/10.1029/2004GC000801)
- D. Krása, V.P. Shcherbakov, T. Kunzmann, N. Petersen, Self-reversal of remanent magnetization in basalts due to partially oxidized titanomagnetites. *Geophys. J. Int.* **162**, 115–136 (2005)
- C. Kutzner, U. Christensen, Effects of driving mechanisms in geodynamo models. *Geophys. Res. Lett.* **27**, 29–32 (2000)
- C. Kutzner, U. Christensen, From stable dipolar towards reversing numerical dynamos. *Phys. Earth Planet. Inter.* **131**, 29–45 (2002)
- C. Kutzner, U. Christensen, Simulated geomagnetic reversals and preferred virtual geomagnetic pole paths. *Geophys. J. Int.* **157**, 1105–1118 (2004)
- C. Laj, J.E.T. Channell, Geomagnetic excursions, in *Treatise in Geophysics*, ed. by M. Kono, vol. 5 (Elsevier, Amsterdam, 2007), pp. 373–416
- C. Laj, A. Mazaud, R. Weeks, M. Fuller, E. Herrero-Bevera, Geomagnetic reversal paths. *Nature* **351**, 447 (1991)
- C. Laj, N. Szeremeta, C. Kissel, H. Guillou, Geomagnetic paleointensities at Hawaii between 3.9 and 2.1 ma: preliminary results. *Earth Planet. Sci. Lett.* **179**, 191–204 (2000)
- C. Laj, C. Kissel, V. Scao, J. Beer, D.M. Thomas, H. Guillou, R. Muscheler, G. Wagner, Geomagnetic intensity and inclination variations at Hawaii for the past 98 kyr from core soh-4: a new study and a comparison with existing contemporary data. *Phys. Earth Planet. Inter.* **129**, 205–243 (2002)
- C. Laj, C. Kissel, A.P. Roberts, Geomagnetic field behavior during the iceland basin and laschamp geomagnetic excursions: a simple transitional field geometry? *Geochem. Geophys. Geosyst.* **7**(3), Q03004 (2006). doi:[10.1029/2005GC001122](https://doi.org/10.1029/2005GC001122)
- L. Lanci, C. Kissel, R. Leonhardt, C. Laj, Morphology of the iceland basin excursion from a spherical harmonics analysis and an iterative bayesian inversion procedure of sedimentary records. *Phys. Earth Planet. Inter.* **169**, 131–139 (2008)
- C.G. Langereis, Excursions in geomagnetism. *Nature* **399**, 207–208 (1999)
- C.G. Langereis, A.A.M.V. Hoof, P. Rochette, Longitudinal confinement of geomagnetic reversal paths as a possible sedimentary artifact. *Nature* **358**, 226–230 (1992)
- C.G. Langereis, M.J. Dekkers, G.J. De Lange, M. Paterne, P.J.M. Van Santvoort, Magnetostratigraphy and astronomical calibration of the: Last 1.1 myr from an eastern Mediterranean piston core and dating of short events in the brunhes. *Geophys. J. Int.* **129**(1), 75–94 (1997)
- R. Leonhardt, K. Fabian, Paleomagnetic reconstruction of the global geomagnetic field evolution during the matuyama/brunhes transition: Iterative bayesian inversion and independent verification. *Earth Planet. Sci. Lett.* **253**, 172–195 (2007)
- R. Leonhardt, H.C. Soffel, A reversal of the earth's magnetic field recorded in midmiocene lava flows of Gran canaria: Paleointensities. *J. Geophys. Res.* **107**(B11), 2299 (2002). doi:[10.1029/2001JB000949](https://doi.org/10.1029/2001JB000949)
- R. Leonhardt, K. Fabian, M. Winklhofer, A. Ferk, C. Kissel, C. Laj, Geomagnetic field evolution during the laschamp excursion. *Earth Planet. Sci. Lett.* **278**, 87–95 (2009)
- S. Levi, H. Audunsson, R.A. Duncan, L. Kristjansson, P.-Y. Gillot, S.P. Jakobsson, Late pleistocene geomagnetic excursion in icelandic lavas: confirmation of the laschamp excursion. *Earth Planet. Sci. Lett.* **96**, 443–457 (1990)
- J. Li, T. Sato, A. Kageyama, Repeated and sudden reversals of the dipole field generated by spherical dynamo action. *Science* **295**, 1887–1890 (2002)
- L.E. Lisiecki, M.E. Raymo, A pliocene-pleistocene stack of 57 globally distributed benthic  $d^{18}O$  records. *Paleoceanography* **20**, PA1003 (2005). doi:[10.1029/2004PA001071](https://doi.org/10.1029/2004PA001071)
- J. Love, Paleomagnetic volcanic data and geometric regularity of reversals and excursions. *J. Geophys. Res.* **103**, 12,435–12,452 (1998)
- J.J. Love, Statistical assessment of preferred transitional vgp longitudes on palaeomagnetic lava data. *Geophys. J. Int.* **140**, 211–221 (2000)
- J.J. Love, A. Mazaud, A database for the matuyama-brunhes magnetic reversal. *Phys. Earth Planet. Inter.* **103**, 207–245 (1997)
- S.P. Lund, M. Schwartz, L. Keigwin, T. Johnson, Deep-sea sediment records of the laschamp geomagnetic field excursion (<41,000 calendar years before present). *J. Geophys. Res.* **110**, B04101 (2005). doi:[10.1029/2003JB002943](https://doi.org/10.1029/2003JB002943)
- G. Masters, G. Laske, H. Bolton, A. Dziewonski, The relative behavior of shear velocity, bulk sound velocity, and compressional velocity in the mantle: implications for chemical and thermal structure, in *Earth's Deep Interior*, ed. by S. Karato, A. Forte, R. Liebermann, G. Masters, L. Stixrude. AGU Monograph, vol. 117 (AGU, Washington D.C., 2000)
- A. Mazaud, An attempt at reconstructing the geomagnetic field at the core-mantle boundary during the upper Olduvai polarity transition (1.66 myear). *Phys. Earth Planet. Inter.* **90**, 211–219 (1995)

- A. Mazaud, 'Sawtooth' variation in magnetic intensity profiles and delayed acquisition of magnetization in deep sea cores. *Earth Planet. Sci. Lett.* **139**, 379–386 (1996)
- A. Mazaud, C. Laj, M. Bender, A geomagnetic chronology for antarctic ice accumulation. *Geophys. Res. Lett.* **21**(5), 337–340 (1994)
- R.T. Merrill, P.L. McFadden, Geomagnetic polarity transitions. *Rev. Geophys.* **37**, 201–226 (1999)
- R. Merrill, M. McElhinny, P. McFadden, *The Magnetic Field of the Earth: Paleomagnetism, the Core, and the Deep Mantle* (Academic Press, San Diego, 1998)
- H. Moffatt, *Magnetic Field Generation in Electrically Conducting Fluids* (Cambridge University Press, Cambridge, 1978)
- F. Nimmo, Energetics of the core, in *Treatise on Geophysics*, ed. by P. Olson, vol. 8 (Elsevier, Amsterdam, 2007)
- N. Nishikawa, K. Kusano, Simulation study of symmetry-breaking instability and the dipole field reversal in a rotating spherical shell dynamo. *Phys. Plasmas* **15**, 082903 (2008)
- N. Olsen, M. Mandea, Rapidly changing flows in the Earth's core. *Nature Geosci.* **1**, 390–394 (2008)
- P. Olson, Gravitational dynamos and the low frequency geomagnetic secular variation. *Proc. Nat. Acad. Sci.* **104**, 20159–20166 (2007)
- P. Olson, H. Amit, Changes in earth's dipole. *Naturwissenschaften* **93**, 519–542 (2006)
- P. Olson, U. Christensen, The time averaged magnetic field in numerical dynamos with nonuniform boundary heat flow. *Geophys. J. Int.* **151**, 809–823 (2002)
- P. Olson, U. Christensen, Dipole moment scaling for convection-driven planetary dynamos. *Earth Planet. Sci. Lett.* **250**, 561–571 (2006)
- P. Olson, U. Christensen, G. Glatzmaier, Numerical modeling of the geodynamo: Mechanisms of field generation and equilibration. *J. Geophys. Res.* **104**, 10383–110404 (1999)
- P. Olson, P. Driscoll, H. Amit, Dipole collapse and reversal precursors in a numerical dynamo. *Phys. Earth Planet. Inter.* **173**, 121–140 (2009)
- P. Olson, R. Coe, P. Driscoll, G. Glatzmaier, P. Roberts, Geodynamo reversal frequency and heterogeneous core-mantle boundary heat flow. *Phys. Earth Planer. Inter.* **180**, 66–79 (2010)
- E. Parker, Hydromagnetic dynamo models. *Astrophys. J.* **121**, 293–314 (1955)
- M. Prévot, P. Camps, Absence of preferred longitude sectors for poles from volcanic records of geomagnetic reversals. *Nature* **366**, 53–57 (1993)
- M. Prévot, E.A. Mankinen, R.S. Coe, S. Grommé, The Steens mountain (Oregon) geomagnetic polarity transition 2. field intensity variations and discussion of reversal models. *J. Geophys. Res.* **90**, 10417–10448 (1985)
- A.P. Roberts, Geomagnetic excursions: Knowns and unknowns. *Geophys. Res. Lett.* **35**, L17307 (2008)
- P. Roberts, S. Scott, On analysis of the secular variation, 1, a hydromagnetic constraint: Theory. *J. Geomagn. Geoelectr.* **17**, 137–151 (1965)
- A.P. Roberts, M. Winklhofer, Why are geomagnetic excursions not always recorded in sediments? Constraints from post-depositional remanent magnetization lock-in modelling. *Earth Planet. Sci. Lett.* **227**, 345–359 (2004)
- J. Rotvig, An investigation of reversing numerical dynamos driven by either differential or volumetric heating. *Phys. Earth Planet. Inter.* **176**, 69–82 (2009)
- D. Ryan, G. Sarson, Are geomagnetic field reversals controlled by turbulence within the Earth's core? *Geophys. Res. Lett.* **34**, L02307 (2007). doi:[10.1029/2006GL028291](https://doi.org/10.1029/2006GL028291)
- G. Sarson, C. Jones, A convection driven geodynamo reversal model. *Phys. Earth Planet. Inter.* **111**, 3–20 (1999)
- A. Schult, Self-reversal of magnetization and chemical composition of titanomagnetites in basalts. *Earth Planet. Sci. Lett.* **4**(1), 57–63 (1968)
- J.C. Shao, M. Fuller, T. Tanimoto, J.R. Dunn, D.B. Stone, Spherical harmonic analyses of paleomagnetic data: The time-averaged geomagnetic field for the past 5 myr and the brunhes-matuyama reversal. *J. Geophys. Res.* **104**(B3), 5015–5030 (1999)
- R. Smittev, F. Busse, Prandtl-number dependence of convection-driven dynamos in rotating spherical fluid shells. *J. Fluid Mech.* **532**, 365–388 (2005)
- B.S. Singer, K.A. Hoffman, R.S. Coe, L.L. Brown, B.R. Jicha, M.S. Pringle, A. Chauvin, Structural and temporal requirements for geomagnetic field reversal deduced from lava flows. *Nature* **434**, 633–636 (2005)
- P.J. Smith, Field reversal or self-reversal? *Nature* **229**(5284), 378–380 (1971)
- B. Sreenivasan, C. Jones, Azimuthal winds, convection and dynamo action in the polar regions of planetary cores. *Geophys. Astrophys. Fluid Dyn.* **100**, 319–339 (2006)
- F. Stacey, *Physics of the Earth* (Brookfield Press, Brisbane, 1992)
- J. Stoner, J. Channell, D. Hodell, C.D. Charles, A 580 kyr paleomagnetic record from the sub-antarctic south Atlantic (ocean drilling program site 1089). *J. Geophys. Res.* **108**, 2244 (2003). doi:[10.1029/2001JB001390](https://doi.org/10.1029/2001JB001390)

- F. Takahashi, M. Matsushima, Y. Honkura, Simulations of a quasi-Taylor state geomagnetic field including polarity reversals on the Earth simulator. *Science* **309**, 459–461 (2005)
- F. Takahashi, M. Matsushima, Y. Honkura, A numerical study on magnetic polarity transition in an MHD dynamo model. *Earth Planets Space* **59**, 665–673 (2007)
- F. Takahashi, M. Matsushima, Y. Honkura, Scale variability in convection-driven MHD dynamos at low Ekman number. *Phys. Earth Planet. Inter.* **167**, 168–178 (2008)
- F. Theyer, E. Herrero-Bervera, V. Hsu, The zonal harmonic model of polarity transitions: a test using successive reversals. *J. Geophys. Res.* **90**, 1963–1982 (1985)
- J.-P. Valet, E. Herrero-Bervera, Some characteristics of geomagnetic reversals inferred from detailed volcanic records. *Compt. Rend. Geosci.* **335**, 79–90 (2003)
- J.-P. Valet, L. Tauxe, B.M. Clement, Equatorial and mid-latitude records of the last geomagnetic reversal from the Atlantic ocean. *Earth Planet. Sci. Lett.* **94**, 371–384 (1989)
- J.-P. Valet, P. Tucholka, V. Courtillot, L. Meynadier, Palaeomagnetic constraints on the geometry of the geomagnetic field during reversals. *Nature* **356**, 400–407 (1992)
- J.-P. Valet, L. Meynadier, Y. Guyodo, Geomagnetic dipole strength and reversal rate over the past two million years. *Nature* **435**, 802–805 (2005)
- J.-P. Valet, G. Plenier, E. Herrero-Bervera, Geomagnetic excursions reflect an aborted polarity state. *Earth Planet. Sci. Lett.* **274**, 472–478 (2008)
- J. Vogt, B. Zieger, K.-H. Glassmeier, A. Stadelmann, M.-B. Kallenrode, M. Sinnhuber, H. Winkler, Energetic particles in the paleomagnetosphere: Reduced dipole configurations and quadrupolar contributions. *J. Geophys. Res.* **112**, A06216 (2007). doi:[10.1029/2006JA012224](https://doi.org/10.1029/2006JA012224)
- J. Wicht, Inner-core conductivity in numerical dynamo simulations. *Phys. Earth Planet. Inter.* **132**, 281–302 (2002)
- J. Wicht, Palaeomagnetic interpretation of dynamo simulations. *Geophys. J. Int.* **162**, 371–380 (2005)
- J. Wicht, P. Olson, A detailed study of the polarity reversal mechanism in a numerical dynamo model. *Geophys. Geochem. Geosyst.* **5** (2004). doi:[10.1029/2003GC000602](https://doi.org/10.1029/2003GC000602)
- J. Wicht, A. Tilgner, Theory and modeling of planetary dynamos. *Space Sci. Rev.* **152**, 501–542 (2010)
- J. Wicht, S. Stellmach, H. Harder, Numerical models of the geodynamo: From fundamental Cartesian models to 3D simulations of field reversals, in *Geomagnetic Field Variations—Space-Time Structure, Processes, and Effects on System Earth*, ed. by H. Glassmeier, H. Soffel, J. Negendank (Springer, Berlin, 2009)
- J. Wicht, S. Stellmach, H. Harder, Numerical dynamo simulations—from basic concepts to realistic models, in *Handbook of Geomathematics* (Springer, Berlin, 2010)
- I. Williams, M. Fuller, Zonal harmonic models of reversal transition fields. *J. Geophys. Res.* **86**(B12), 11657–11665 (1981)
- P. Willis, B. Sreenivasan, D. Gubbins, Thermal core-mantle interaction: Exploring regimes for ‘locked’ dynamo action. *Phys. Earth Planet. Inter.* **165**, 83–92 (2007)
- H.-U. Worm, A link between geomagnetic reversals and events and glaciations. *Earth Planet. Sci. Lett.* **147**, 55–67 (1997)